GFZ
Helmholtz-Zentrum
POTSDAM

Originally published as:

Toledo Zambrano, T. A., Jousset, P., Maurer, H., Krawczyk, C. (2020): Optimized Experimental Network Design for Earthquake Location Problems: applications to geothermal and volcanic field seismic networks. - Journal of Volcanology and Geothermal Research, 391, 106433.

Optimized Experimental Network Design for Earthquake Location Problems: applications to geothermal and volcanic field seismic networks

Toledo T.[1,3], Jousset P.[1], Maurer H.[2], Krawczyk C.[1,3]

[1]*GFZ German Research Center for Geosciences*

[2]*Swiss Federal Institute of Technology, Zürich, Switzerland*

[3]*TU Berlin*

2020

Abstract

We constructed a network optimization scheme based on well established survey design tools to design and qualify local and regional microseismic monitoring arrays dedicated for geothermal exploration and volcano monitoring. The optimization routine is based on the traditional minimization of the volume error ellipsoid of the linearized earthquake location problem (D-criterion) with the twist of a sequential design procedure. Seismic stations are removed one by one to obtain networks for constraining the locations of multiple hypothetic earthquakes with varying local magnitudes. The sequential approach is simple and allows the analysis of benefit/cost relations. Cost curves are computed for all hypothetic events to reveal the minimum optimal number of stations given specific design experiment objectives.

The scheme is first demonstrated on three test design experiments. Later, we use the routine to augment an existing seismic network for monitoring microseismicity in a geothermal field in NE Iceland (Theistareykir). The resulting 23 station network would become the backbone of a reservoir behavior and exploitation activity study. Hypothetic event locations and magnitude relations are taken from a previous regional seismicity study and coincide with geothermal injection and production areas. Sensitivities are calculated with a known 1D velocity model profile using a finite-difference back-ray tracer, and body wave amplitudes are computed from known local magnitude relations. Finally, expected earthquake location accuracies are calculated via multiple Monte Carlo experiments.

The design routine is later used to qualify an existing seismic network located in SW Iceland (Reykjanes). The seismic array is reduced to strategic positions, and benefit and expected accuracies are quantified to observe whether costs could have been optimized had a previous network design

2

experiment been performed.

Overall, we explore quick and flexible tools for designing and qualifying networks for many applications at various scales.

Introduction

Since the mid 70s, the identification of economically attractive reservoirs and their exploitation for geothermal heat energy have been the aim of numerous projects worldwide (*Tester et al.*, 2006; *Dyer et al.*, 2008). Parameters such as heat source, reservoir, and preferential fluid pathways geometries, the availability and characteristics of underground fluids, and the knowledge of the recharge area are some of the main targets for the exploration of both conventional and enhanced geothermal systems (EGS). These parameters rarely show surface manifestations, and are therefore mostly assessed by geophysical techniques such as microseismic monitoring.

Several studies have shown that geothermal and volcanic systems are usually associated with high levels of natural and/or induced microseismic activity (e.g. Soultz-sous-Forêts (*Cuenot et al.*, 2008), Hengill (*Jousset et al.*, 2011), Basel (*Majer et al.*, 2007), Merapi volcano (*Surono et al.*, 2012), Reykjanes (*Blanck et al.*, 2018, *this issue*), Krafla (*Foulger et al.*, 1983)).

These events are good indicators of the active processes in the subsurface. Accurate event location can potentially help identify the reservoir boundaries; the shape, size, position, and/or growth of active fractures or faults (*Philips et al.*, 2002); and, when correlating the seismicity evolution with time, the migration patterns of injection fluids. Well-constrained events also improve results of further seismic studies such as earthquake tomography, attenuation and anisotropy structural analysis, and source mechanism determination with first arrival wave polarity (e.g. *Blanck et al.*, 2018, this issue) for an overall better understanding of a geothermal field and/or volcanic hazard

3

assessment. In the best case scenario, high precision micro-earthquake locations serve as guides for further drilling and development of a geothermal field (e.g. *Jousset et al.*, 2018, this issue). In a similar way, volcanic hazard studies can be enhanced with better seismic event precision (e.g. *Surono et al.*, 2012).

High precision hypocentral parameters are the aim of most passive microseismic studies and considerable effort is currently dedicated to develop standardized data-processing and inversion techniques. These methods range from ray-based (e.g. *Aki and Richards*, 1980; *Kissling et al.*, 1994) and grid search methods (e.g *Sambridge and Kennett*, 1986, 2001; *Lomax*, 2005), to wave-field back-propagation (e.g. *McMechan*, 1982; *Witten and Artman*, 2011) and waveform stacking (e.g *Kao and Shan*, 2007; *Cesca and Grigoli*, 2015), among others. Ray-based or arrival time inversion techniques with travel time picking are to this day the most common choice in microseismic experiments given their formulation simplicity, their relatively fast computation despite the large amounts of data, the availability of inversion packages, and the proven results in numerous case studies. Several of these standard automated location routines rely on Geiger's algorithm (*Geiger*, 1912), where the location is derived by carrying out an inversion that iteratively minimizes observed and synthetic travel times of body waves (*Aki and Richards*, 1980). For simplicity and inversion stability, event location is usually first performed using a 1D reference velocity model. This assumption can limit the location accuracy, given the systematic biases that are introduced by 3D velocity changes. This effect is normally alleviated by including source and/or station correction terms and/or jointly inverting the travel time data for both hypocenters and velocity structure in local earthquake tomography studies (e.g. *Ellsworth* (1977); *Roecker* (1981); *Eberhart-Phillips* (1990); *Thurber* (1992); *Kissling et al.* (1994); *Michelini* (1995)).

It has been pointed out by several authors that the success, reliability, and accuracy of the

results strongly depend on acquired data quality mainly given by the number of available phases, accurate picking (if needed) (*Pavlis*, 1986), and network geometry (*Kijko*, 1977; *Uhrhammer*, 1980; *Rabinowitz and Steinberg*, 1990). Although we have limited influence on the micro-earthquake occurrence, we can maximize the information content of an experiment by designing optimal network configurations or by selecting an optimal subset of an existing dense dataset (e.g. *Maurer et al.*, 2010). Ideally one can think of improving results precision by using a large number of seismometers, in practice however, geothermal exploration and seismic monitoring in general is strongly constrained by budget. On top of that, no additional information can ever compensate missing or inadequate data required for resolving a target parameter, hence the critical importance of the survey design choice.

The usual procedure in geothermal exploration or volcano monitoring is to deploy a number of seismometers (6 or more) covering a prospect area or volcano, and record continuously over a period of time at sampling rates higher than 50 Hz. Often the seismic network is designed following a heuristic approach with some basic guidelines: the expected microseismic events should be located within the array forming an azimuthal gap of less than $\sim 180°$ (*Valtonen et al.*, 2013), and the average inter-station spacing should be of the average hypocentral depths.

In some cases, standard designs involve specific configurations required for existing inversion and analysis tools. The later choice can be quite restrictive when encountering field and/or instrumentation constrains. Heuristic design can also lead to difficulties in evaluating potential error estimations. Several inversion tests would be needed to find an adequate design that effectively minimizes potential errors, leading to a considerably large computational cost.

Alternative network design strategies have been introduced in the framework of experimental design (ED) for a variety of applications (e.g. *Glenn and Ward*, 1976; *Uhrhammer*, 1980; *Jones*

and Foster, 1986; *Maurer and Boerner*, 1998; *Curtis*, 1999; *Wilkinson et al.*, 2006; *Coles and Curtis*, 2011a; *Kraft et al.*, 2013; *Nuber et al.*, 2017). The main concept is to minimize (or maximize) an objective function representing optimum network performance, which is in many cases related to the eigenvalue content of the linearized inverse earthquake location problem. One popular functional for the earthquake location problem is the *D-criterion* first implemented by *Kijko* (1977) and later exploited by *Rabinowitz and Steinberg* (1990) to monitor a single point source using the DETMAX algorithm (*Mitchell*, 1974). Later *Steinberg et al.* (1995) extended these principles to obtain networks dedicated to monitor fault lines and multiple seismic sources by introducing a multi-source objective function. The *D-optimal* concept for event location network design is also implemented in the software program OPTINET (*Shimsoni et al.*, 1992).

The *D-criterion* is however only applicable in linearized design problems. Geoscientific experiments on the other hand exhibit a complex non-linearity which only increases with the number of optimizing parameters and observables. This makes nonlinear optimization still very prohibitive at large scales due to its large computational demand, however some efforts in this direction have been made with promising results. *Coles and Curtis* (2011a), for example, presented a practical approach for fully non-linear Bayesian statistical experimental design by introducing a generalization of the *D-criterion* which they called D_N optimization. This function benefits from linearized methods to make the optimization computationally feasible in comparison to other non-linear approaches. They applied the algorithm to construct a seafloor microseismic network for monitoring an offshore petroleum field and compared its performance with a network acquired with linearized Bayesian sequential design, with better results using their method.

Hardt and Scherbaum (1994) studied the potential for multi-purpose designs addressing objectives such as tomography, focal mechanisms, and source-parameter estimation for an aftershock

experiment. Their work uses a simulated annealing approach (*Kirkpatrick et al.*, 1983) that reduces a synthetic temperature to search for the global minimum of the objective function. Their results primarily point out that different research objectives require different network configurations. Later *Kraft et al.* (2013) extended this algorithm to include the possibility of using 3-D velocity models by adding a finite-difference ray tracer to compute travel-times. They also introduce the construction of event detection thresholds by using the Brune source model (*Brune*, 1970, 1971) to compute body-wave amplitudes and compare them to local noise level amplitudes for augmenting a microseismic network in northern Switzerland (*Kraft et al.*, 2013).

Although global optimizers provide optimal configurations, its use may require extensive computations as different initial configurations would be needed to check for the stability of the solutions. Moreover, global optimizers can be quite restrictive when addressing changes in the theoretical station positions due to field conditions, and many more calculations would be then necessary to produce an alternative station configuration that accounts for these new constrains. These facts motivated *Curtis et al.* (2004) to use a sequential design approach for a 2D microseismic monitoring example with sources placed inside a borehole. The idea consisted of removing receiver positions that represent redundant data in a stepwise fashion. In this paper we shall explore a similar approach in 3D for constructing and qualifying passive seismic networks for geothermal exploration purposes. This sequential optimization concept not only reduces the computation time for network design but it also facilitates addressing the benefit/cost question, which is oftentimes overlooked.

One main goal of this study is to apply fast and well-established linearized sequential survey design tools to a new problem: constructing and qualifying microseismic arrays dedicated to monitor geothermal operations. Therefore, after introducing a brief theoretical background for

earthquake location problems and relevant concepts of experimental design theory, we present the used algorithm with the particular emphasis of treating large amounts of hypothetical sources of varying local magnitudes to obtain optimal positions for a given number of seismic stations. The chosen scheme is robust, simple, and addresses concepts like benefits and costs. It is also particularly useful for qualifying and augmenting networks with existing stations. We therefore first introduce three simple test cases to demonstrate the chosen approach. Later, we present the two case studies where the algorithm was used to augment (Theistareykir case study), and test the network quality of an existing array (Reykjanes case study).

Although global optimality cannot be guaranteed by sequential methods -whether the metric used is linearized or non-linear-, the technique hereby explored arrives to quick designs with good performance nonetheless. Linearized sequential design poses less computational costs which makes these techniques more efficient in cases where quick designs are needed such as post-earthquake aftershock studies. It could also provide a framework for potential design-during-deployment (DDD).

The word "linearized" here and throughout this manuscript refers to the fact that the quality metric used to assess each design relies on a linearized information measure. Hence, even if a Bayesian formulation -which includes an a priori distribution of models- is used, such a measure can only provide an approximation to the true measure of information expected to be provided by each design. Whether or not the globally optimal experiment under that information measure is found has nothing to do with the measure, and therefore has nothing to do with linearization.

Global optimality can be obtained when using linearized design quality metrics if a global optimization algorithm is used (such as a simple grid search over design space). By contrast, *Guest and Curtis* (2009) use sequential methods to design experiments using fully nonlinearized quality

measures; so although for each design their quality metric will give a more robust assessment of the amount of information than linearized metrics (but of course more costly to evaluate), the sequential methods that they applied, while fast to converge, will not in general find the globally optimal design under that metric.

Background theory and synthetic examples

Basic principles of earthquake location and inverse theory

Micro-earthquake location is a classical nonlinear inverse problem that aims to obtain a set of model parameters $\mathbf{m}$ (event position coordinates $\mathbf{x}_o$, $\mathbf{y}_o$, $\mathbf{z}_o$, and origin time $\mathbf{t}_o$) from observed data $\mathbf{d}^{obs}$ (P and S wave arrival times $\mathbf{t}_p$ and $\mathbf{t}_s$) assuming a mapping operator $\mathbf{G}$ that relates them. The linearized system of equations representing the forward problem is expressed as:

$$\mathbf{d} = \mathbf{Gm} \tag{1}$$

where G corresponds to the true physical processes in the subsurface when it relates a true model of the subsurface $\mathbf{m}^{true}$ with $\mathbf{d}^{obs}$. In a similar fashion any set of predicted data $\mathbf{d}^{est}$ can be calculated using an estimated set of model parameters $\mathbf{m}^{est}$ assuming a known forward operator or data kernel G. In the event location problem, G is comprised by the sensitivities of travel times with respect to the hypocentral coordinates and the origin time. These sensitivities are calculated in this work by using *Podvin and Lecomte* (1991) finite-difference time-field calculations and a back-raytracing routine.

One usual procedure to tackle the inverse problem is to iteratively compute forward modeled data $\mathbf{d}^{est}$ and compare it to the observed dataset $\mathbf{d}^{obs}$ such that the misfit between the two is minimized (*Tarantola*, 2005). To achieve a better search of the global minima, the problem is commonly solved by adding regularization constrains that tackle instabilities due to data uncertainties (*Levenberg*, 1944; *Marquardt*, 1963). The damped least-squares solution to the inverse problem of Eq. 1 is given by:

$$\mathbf{m}^{est} = (\mathbf{G}^T\mathbf{G} + \gamma\mathbf{I})^{-1}\mathbf{G}^T\mathbf{d} \qquad (2)$$

where γ corresponds to the damping factor, and *I* is an *NxN* identity matrix with *N* being the number of model parameters contained in $\boldsymbol{m}$ (4 for this case). Square matrix $\mathbf{G}^T\mathbf{G}$ is often near singular, and inversion stability strongly depends on its ability to be inverted. The reader is referred to *Menke* (2012) and *Lee and Stewart* (1981) for extended relevant derivations.

Experimental survey design: the *D*-criterion

The main goal of experimental survey design is to select a network geometry or data subset that would minimize the computational and/or acquisition costs while optimizing the benefit of an inversion problem (*Maurer et al.*, 2010). This benefit or "goodness" can best be described in terms of the potential information content that can be obtained from a dataset, namely the eigenvalue content ($\lambda_i : i = 1, ..., N$) of matrix $\mathbf{G}^T\mathbf{G}$ (*Curtis*, 2004).

One important property of eigenvalue content is its relationship to error propagation. Errors in the data space propagate into the solution $\mathbf{m}^{est}$ with an amplification of $1/\lambda_i$, parallel to their corresponding eigenvector. This means that for small eigenvalues the propagation error can be quite large if not making the solution unstable altogether (ill-conditioned problem). As a matter of fact, the covariance matrix of the solution to Eq. 2 is given by (*Menke*, 2012):

$$cov(\mathbf{m}) = \sigma^2(\mathbf{G}^T\mathbf{G})^{-1} \qquad (3)$$

where σ^2 corresponds to the variance of onset-time determination. Assuming a constant σ^2, the shape of the precision ellipsoid is given by eigenvectors and eigenvalues of $1/(\mathbf{G}^T\mathbf{G})$ and its

volume is proportional to $1/\det(\mathbf{G}^T\mathbf{G})$ (*Flinn*, 1965; *Buland*, 1976).

Several design quality measures based on matrix $\mathbf{G}^T\mathbf{G}$ have been proposed, compared, and analyzed in previous experimental design works (e.g. *Curtis*, 1999, 2004; *Maurer et al.*, 2010). However one popular measure in earthquake location problems is given by the determinant of $\mathbf{G}^T\mathbf{G}$, also known as the *D-criterion* due to its sensibility to the entire eigenvalue spectrum (*Kijko*, 1977; *Rabinowitz and Steinberg*, 1990; *Hardt and Scherbaum*, 1994). After testing different quality measures based on the *D-criterion*, we chose to work with a modified version of the multi-source function defined by *Rabinowitz and Steinberg* (1990) for best results. We thus define our quality measure Θ as:

$$\Theta = \sum_{i=1}^{N} \gamma_i \log\left(\frac{1}{\det(G_i^T G_i) + \delta}\right) \tag{4}$$

where N stands for the total number of earthquakes, and γ_i corresponds to a weighting factor assigned to each event i ($\gamma_i = 1$ for all events studied in this work). In a Bayesian framework, weights γ_i could be regarded as prior probabilities for the hypocenters (*Chaloner and Verdinelli*, 1995). In this study however, the weights reflect a combination of a prior probability and an event importance (*Steinberg and Rabinowitz*, 2003). We introduce a small value δ in Eq. 4 to stabilize the optimization procedure for cases where the determinant would be zero (under-determined case). With this objective function we would in some sense minimize for the confidence ellipsoid volume of all events.

Sensitivities in $\mathbf{G}$ are solely related to the survey design. Hence the "goodness" of matrix $\mathbf{G}^T\mathbf{G}$ can be maximized by selecting the source-receiver configuration that would result in the highest eigenvalue content (minimizing quality measure Θ). In a destructive sequential design framework, $\mathbf{G}$ is first comprised of all possible sensitivity entries, namely all detecting station positions. Later,

Θ values are calculated after removing each recording sensor. These values are then compared and the position associated to the minimum Θ value (possibly redundant information) is removed. This process is carried out in a step-wise fashion depleting the *potential deploying area*.

Event detectability

To address the design problem of defining this *potential deploying area* we examine the event detectability in space (e.g. *Hardt and Scherbaum*, 1994; *Coles and Curtis*, 2011a; *Kraft et al.*, 2013). The original amplitude of a seismic phase is influenced mainly by the following factors: magnitude, wave propagation effects (namely geometrical spreading and attenuation), and source processes. The first two factors are addressed in this work only in an approximate manner. Then, events are detected at a point only when their recorded amplitudes are greater than the noise levels at that recording point.

We use the empirical local magnitude-attenuation relation used by the national seismic network in Iceland (South Iceland Lowland or SIL system) to compute recorded amplitudes (*Jakobsdóttir*, 2008):

$$M_L = \log_{10} A + 2.1 * \log_{10} \Delta - 4.8 \tag{5}$$

Eq. 5 is based on the maximum peak-to-peak amplitude in a 10 seconds interval around the S-wave at all stations, where Δ represents the earthquake-station distance in km, and A is the maximum velocity amplitude of high-pass filtered waveforms with cutoff frequency at 2Hz and a scaled response of a Lennartz 1Hz sensor and a Nanometrics RD3 digitizer.

To construct a detection radius, A is chosen to match a minimum amplitude above an expected noise level. In this work we assume rms noise amplitudes of around 42 nm/s throughout the

available space. This rms ground velocity amplitude (v_{rms}) was obtained using the following relation (*Bormann*, 1998):

$$v_{rms} \approx \sqrt{2 \cdot \langle P_a/\omega^2 \rangle \cdot (f_2 - f_1)} \tag{6}$$

where P_a corresponds to the most probable noise level at a given frequency interval obtained from the probabilistic power spectral density (PPSD) for ground acceleration (*McNamara and Buland*, 2004) at a given station. Then $\langle P_a/\omega^2 \rangle$ corresponds to the mean converted ground velocity function over a frequency range between f_1 and f_2. Finally, ω stands for the angular frequency. In this work we chose a seismic station located north to the Krafla region in Iceland (*Lees*, 2004), computed its corresponding PPSD using Obspy (*Beyreuther et al.*, 2010), and calculated the v_{rms} associated to frequencies above 2 Hz.

Then we selected a large signal to noise ratio (SNR $\approx$ 15) for detection threshold construction. Authors like *Hardt and Scherbaum* (1994) point out that a SNR of 3 should be enough to detect a seismic phase onset. However given that only the maximum amplitude in a time window is taken into consideration for the detection, as well as the uncertainties of lateral noise amplitude variations, we chose a much more conservative SNR value to construct the detection thresholds. The *potential deploying area* would then correspond to the region within this detection radius.

Detectability is not the main focus of this work and is therefore roughly addressed. Amplitudes, noise, and magnitude values used are regarded as estimates only, and are merely utilized to define a region to include stations for both the test cases and Case study I, which corresponds to a region neighboring Krafla. It is advisable, where there would be available preliminary seismic data, to compute laterally-variant noise estimates as done by *Kraft et al.* (2013), as well as refining variable values of SNR. Hence, we recommend to update detection models and repeat optimizations

once more information on the target sites becomes available. We have also not accounted for different radiation patterns given the typically unknown source parameters in unexplored areas. We encourage to explore this variable when more information is available.

Test Case A: survey design for a single source

To demonstrate the use of the destruction sequential survey design algorithm (DSSD), Fig. 1 shows the construction of a 5 (Fig. 1a) and a 115 (Fig. 1b) station network for locating a single event of M_L 0.8 and 3 km depth in a homogeneous media of constant P-wave velocity (V_p) of 4 km/s. The possible station locations consist of the nodes of a triangular grid with mean spacing of 3.5 km, obtained using the *Persson and Strang* (2004) open-source mesh generator. The triangular mesh was chosen in accordance with the work of *Kraft et al.* (2013).

First, we construct the *potential deploying area* (region within dashed red lines in Fig. 1a and Fig. 1b) for the given event and the sensitivity matrix **G** for the total number of recording sensors (115 for this case). Next, we remove one station and calculate the quality value Θ for the remaining 114 station network. We put this station back into the network, remove another station, and calculate Θ again. This process is carried out for all recording stations to obtain a list of 115 Θ values. Then we permanently remove the point with lowest associated Θ, and assign to it the last placement number position (115 in this case). In other words we search for the station whose removal would worsen the network quality the least, and would therefore be the last one we would need to place for optimally constraining the hypocenter. Next, we repeat this procedure with the remaining 114 stations to look for the second to last placement number position. This process is repeated until the total 115 available receivers are removed (triangles in Fig. 1b) and the full placement order sequence is created (colorbar in Fig. 1a and Fig. 1b). Notice how when displaying the first 4
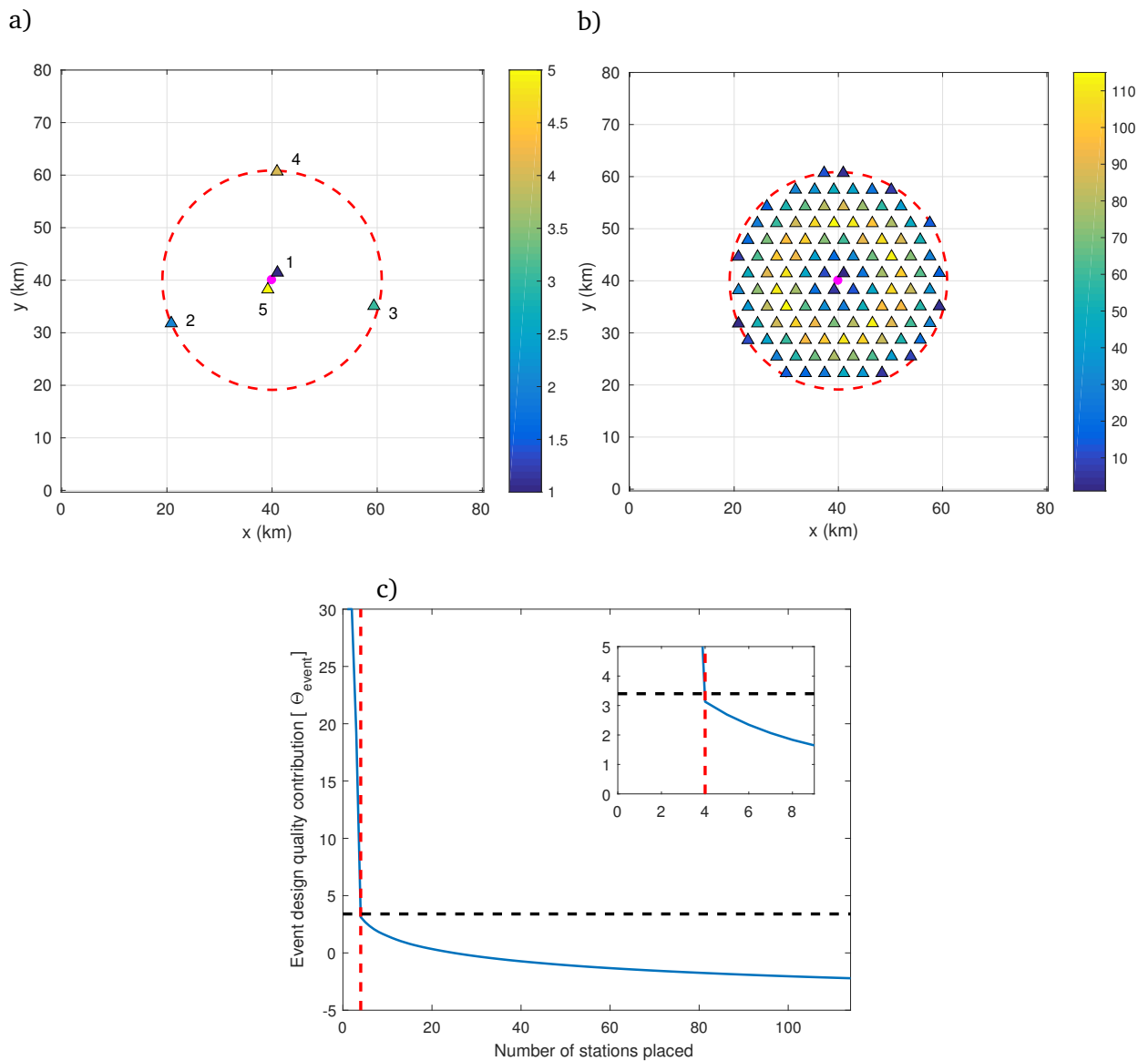
Figure 1: Test case A. Survey design example for an event at 3km depth with M_L 0.8. a) 5 station setup. b) 115 station setup. The colorbar expresses the order of placed stations. c) Design quality or "goodness" of the survey setup for each number of placed stations. The dashed red line represents station point 4, and the horizontal dashed black line the limit of $\Theta = 3.4$.

seismic stations of the placement sequence (Fig. 1a), the distribution has a quadripartite geometry

in accordance with results of *Rabinowitz and Steinberg* (1990) and *Hardt and Scherbaum* (1994),

with the closest point to the epicenter as the very first station position. When further adding a

fifth sensor, notice how this receiver is placed again at a position close to the epicenter. Given the

proximity of this location to Station #1, this position can be regarded as redundant information. In the framework of *D*-optimality this clustering or redundance can be interpreted as a high regional importance (*Kraft et al.*, 2013). In this particular case, the double positioning is the result of no station candidate located right above the earthquake epicenter. It is for this reason that the resulting station position sequence must be carefully assessed before ultimately defining a network. Later, after displaying the entire sequence (Fig. 1b) we clearly see that the first deployed stations (in darker blue) correspond to those close to the source and to those bordering the detection radius limit.

Fig. 1c shows the variation of the design quality value Θ after using *-n* station positions. Low Θ values indicate good array quality. This curve is a good representation of the benefit/cost relations of the survey design problem. The cost is interpreted as the number of placed stations and the benefit is defined by the value of Θ itself, proportional to the logarithm of the resulting confidence ellipsoid volume. Notice how this value decreases rapidly with the first 4 stations, after which this decrease does not vary significantly. This means it takes only a few optimally positioned stations to reach good network quality. We define a benefit threshold of $\Theta = 3.4$ for this case (dashed blue line) to select a minimum number of stations (4). Using additional receivers will further decrease the confidence ellipsoid volume and it would then be up to the user to decide the number of needed stations to meet the objectives of an experiment, however some attention must be given to potential station clustering. Notice also after placing enough stations, this decrease is not significant, hence the benefit/cost curve tends to flatten with large number of stations.

Though the proposed algorithm can potentially use both P-wave (*Vp*) and S-wave (*Vs*) velocities for building the sensitivity matrix, we chose to work only with *Vp*. Errors in *Vs* can considerably influence towards constructing a suboptimal station network. On one hand *Vs* is typically lower

than *Vp,* hence providing higher sensitivities to t_S measurements. At the same time, S-wave picks are often hard to acquire, especially in the presence of noisy data. *Gomberg et al.* (1990) point out that although S-wave data can significantly improve the accuracy of hypocenter location and reduce the trade-off between origin time and source depth, incorrect estimates can also significantly degrade it. In this work we therefore consider S-wave travel-time measurements merely as added values improving the location accuracies at a later stage however not in the design experiment.

Test Case B: small multi-event survey design

In this example we will build a seismic network dedicated to constrain 3 known event targets at a depth of 3 km with varying local magnitudes (M_L 0.8, 0.6, and 0.5). As an initial step, and similar to the previous example, we construct the *potential deploying areas* for all three events. On a second step, the multi-event quality measure Θ is computed after removing each recording station in the system, while carefully accounting for their contribution only to the events that are detected by them. Values are then compared and the station that effectively minimizes Θ is removed. As in the previous exercise, this procedure is repeated until all 231 stations are removed.

Fig. 2a and Fig. 2b show the resulting 12 and 231 station networks, respectively. Similar to Test Case A, the first stations of the placement order sequence are those close to the event epicenters and those close to the detection boundaries (dark blue triangles). However, no perfect quadripartite geometry is provided for all the events (Fig. 2a). This failure to arrive to a perfect 4 station geometry occurs when *potential deploying areas* overlap (as is the case of $Event_1$ and $Event_2$). The multi-source objective function will naturally favor these areas given that their contribution to more than one event will reduce Θ most (hence the deep blue triangles all through this region in Fig. 2b). Overlapping areas will be even more favored when these regions are considerably
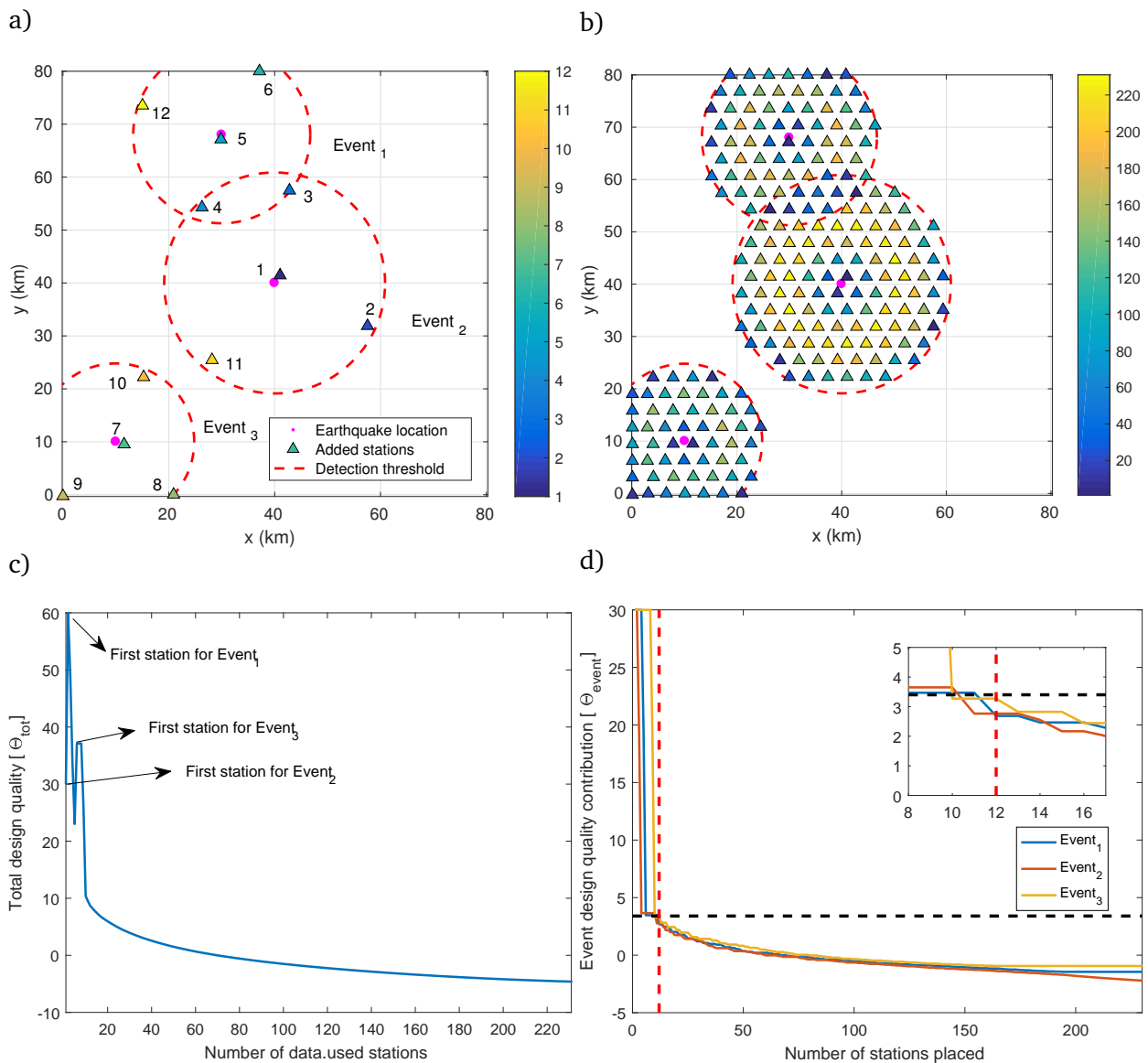
Figure 2: Test case B. Survey design example for three events 3 km deep. Events have M_L 0.8 (center), 0.6 (top), and 0.5 (bottom left). a) 12 station setup. b) 231 station setup. The colorbar expresses the order of placed stations. c) Total design quality or "goodness" of the survey setup after progressively placing stations. d) Design quality contribution per event for the whole experiment. The dashed red line represents station point 12, and the horizontal dashed black line the limit of $\Theta_{event} = 3.4$.

large. In these cases, stations would be very hardly placed outside of them, yet it will keep the

pattern of putting stations close and far from the epicenters within them. The algorithm could

then potentially return a poorer convergence to a perfect quadripartite geometry. To obtain better

19

geometries for particular events, one can assign them higher weighting values γ_i (Eq. 4).

The benefit/cost curves, namely the total design quality values Θ_{tot} and the individual event contributions Θ_{event}, are shown in Fig. 2c and Fig. 2d respectively. Design quality curve Θ_{tot} reveals two marked peaks which correspond to the points where the routine has placed the first station at an event deploying area (e.g. station # 7 would be the first sensor placed for Event$_3$). The contribution of a single sensor at a deploying space yields $\Theta_{event} = 30$, which is result of the sole influence of δ in an under-determined case (Eq. 4). An increase of 30 in Θ_{tot} is also visible at these points, hence the peaks in the curve. Naturally, before this first station is introduced no contribution to Θ_{tot} or Θ_{event} is made for this event. Placing a second station would barely reduce this value of 30, for which Θ_{tot} and Θ_{event} hardly decrease (still under-determined case). It is only after introducing the third and fourth stations at a deploying space (reaching an even-determined case) that Θ_{event} is reduced to a value between 3 and 4 (Fig. 2d). If we now define a benefit limit per curve of $\Theta_{event} = 3.4$ (dashed blue line), we would then require the 12 stations shown in Fig. 2a.

Test Case C: large multi-event survey design

So far, we have addressed the network design for locating a single or very few known events, in practice however, microseismicity studies for geothermal monitoring typically present hundreds if not thousands of events. The next question is how to construct a seismic network for optimizing a large number of earthquakes. Like the previous two cases we assume a constant Vp of 4 km/s throughout the domain, but this time we introduce 1089 events of M_L 0.5 and depth of 3 km placed in a grid-like manner every 2.5 km in x and y directions.

Similar to the previous exercises we use the DSSD algorithm to construct the station placement

sequence and their associated quality curves. Fig 3a and Fig. 3b show the resulting 100 and a 598 station networks, respectively, and Fig. 3c and Fig. 3d depict the experiment design qualities Θ_{tot} and Θ_{event}. Notice the overall decreasing trend of Θ_{tot} after first reaching a maximum at ≈ 26 stations. This is the point where most events have at least one seismic station in their *deploying area* ($\approx 60\%$ of stations).

Once more, from the cost curve (Figure 3d) we may observe and select a number of stations that would best constrain most of the 1089 events. It is important to note that constraining all events will be very expensive and at times not realistic. More often than not, we should be ready to sacrifice the benefit or location accuracies of some events for cost reasons. In this case, we select 100 stations (Fig. 3a), given that most event cost curves reach a benefit $\Theta_{event} \leq 3.4$ (horizontal black dashed line in Fig. 3d). In the resulting network, receivers are scattered in a quasi-regular way throughout the domain with few stations placed at the boundaries. The overall station sequence presents a very similar quasi-regular behavior in Fig. 3b.
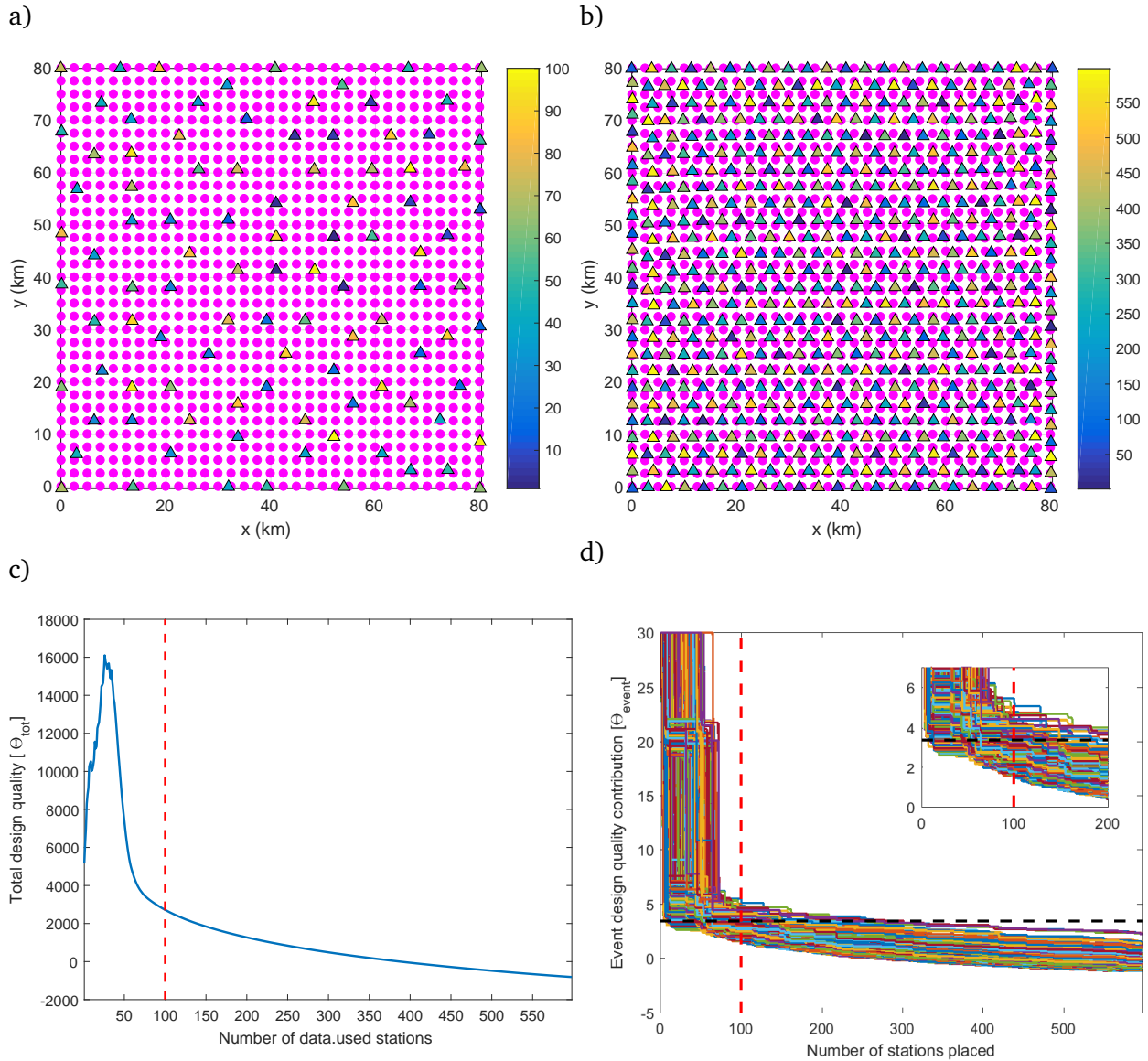
Figure 3: Test case C. Survey design example for multiple events of M_L 0.5 located at 3 km depth. Pink points indicate epicenter locations and triangles stand for station locations. The colorbar expresses the order of placed stations. a) 100 station setup. b) 598 station setup. c) Total design quality or "goodness" of the survey setup after progressively placing stations. d) Design quality contribution per event for the whole experiment. The dashed red line represents station point 100, and the horizontal dashed black line the limit of $\Theta_{event} = 3.4$.

Case study I: Theistareykir geothermal field

Theistareykir is a high temperature geothermal field located in NE Iceland that extends from the Öxarfjördur Bay to the center of the country and is associated to the Bjarnafell volcano (Fig. 4). It is characterized by a set of large normal faults that strike N22°E with maximum offset of around 200-300 meters, and various rift fissures (*Sveinbjornsdottir et al.*, 2013). This geothermal field has undergone intermittent exploration (1972-1974 and 1981-1984) and monitoring (1991-2000) to assess its capabilities for drilling and production (*Ármannsson*, 2008), and is currently under the administration of Landsvirkjun, the national power company of Iceland. Between 2002 to 2008 seven deep wells were drilled with depths of 1723 m to 2799 m, and up to 8 additional wells were included by the end of 2017 (*Landsvirkjun*, 2016). Many of these wells were drilled almost horizontally and the power plant is producing at a capacity of 90 MW since spring 2018.

According to a Landsvirkjun report on seismic data recorded between November 1st 2016 and March 31st 2017 (*Blanck et al.*, 2017), most of the activity is clustered in the form of vertical chimneys close to the production zone. The report shows a total of 140 earthquakes located mainly at depths between 2 and 5 km with an array consisting of mainly 4 seismic stations in the close vicinity: 1 from the national seismic array (SIL system) and 3 operated by Iceland Geosurvey (ISOR) for Landsvirkjun. These events have mostly local magnitudes of 0.5 and higher, exhibiting a Gutenberg-Richter b-value relation of 2.16. *Blanck et al.* (2017) interpreted that the large amount of higher magnitude events could be the result of either a strong crust at the site, or the side-effects of a small seismic network.
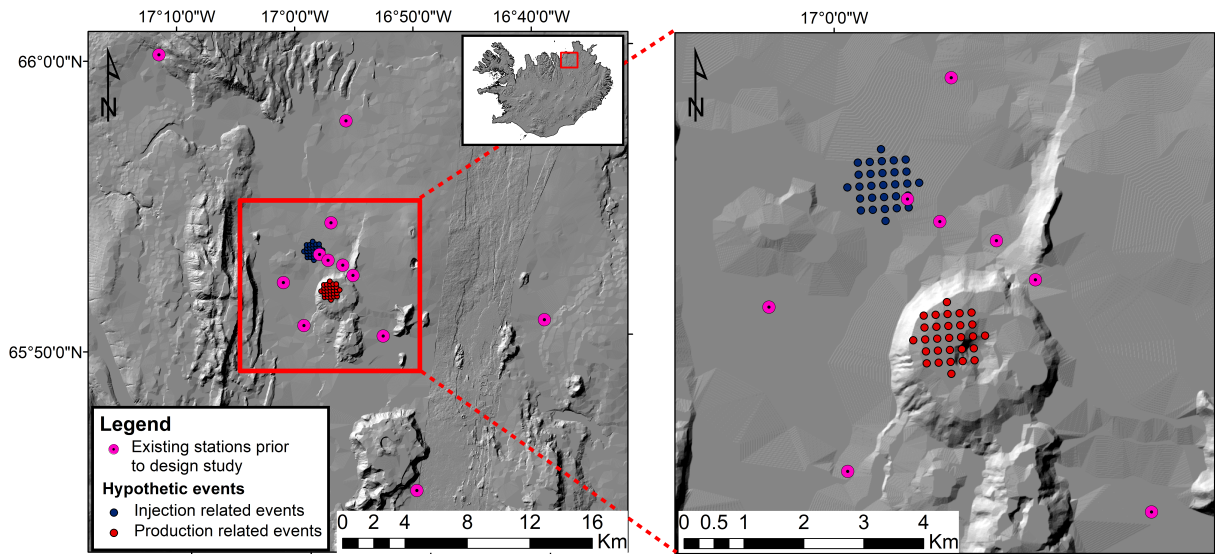
Figure 4: Initial receiver positions and synthetic epicenters defined prior to the design study.

Experimental design setup, results and discussion

To better understand the structures and behavior of the reservoir, a seismic network consisting of 12 broadband stations will be augmented to monitor the Theistareykir geothermal field (Fig. 4). This network is part of a larger deployment effort to monitor the exploitation activity with an array of multi-parameter stations including gravimeters, GNSS receivers, and seismic sensors (*Jousset et al.*, 2018, EGU abstract). From the seismic stations depicted in Fig. 4, seven are permanent stations belonging to the Icelandic Meteorological Office (IMO) and Iceland Geosurvey (ISOR), and five stations belonging to the German Research Center for Geosciences (GFZ) will be fixed at the gravimeter station positions. In this exercise an additional 11 seismic station positions has been defined for a total of 23 receivers across the geothermal field.

Following the proposed sequential survey design recipe, we first specify the target areas where we may expect future microseismic events. These regions correspond to the production and in-

jection zones depicted by the red and blue cluster of points, respectively (Fig. 4). As a next step we generate a synthetic earthquake catalog (196 events) using these points as epicenters, and the depth and magnitude distributions of the catalog studied by *Blanck et al.* (2017) (Fig. 5). We chose to focus on local magnitudes between 0.5 and 0.8. Fig. 5a depicts the 1D P- and S-wave velocity profiles typically used by the IMO for earthquake locations, though for the design experiment we shall once more only use the 1D P-wave velocity profile.

As in the first test cases the domain is discretized to a 2D triangular grid with node distances of roughly 3.5 km. After defining *deploying areas* for each event, we perform the DSSD algorithm two times: the first time using only the 12 deployed stations as "potential location points", and the second one right after, to account for the remaining positions in the full *deploying space*. Results of the first survey design experiment provide an order of importance of the fixed stations positions and determine which are the critical ones among them. The second exercise is performed to augment the array.

Theistareykir experimental survey design

Fig. 6a and Fig. 6b show the resulting 23 and 135 (complete) station networks. Notice how on the first network the selected stations are located at the outer limits of *deploying areas* with smaller detection radii. However, few stations are anyways placed at the northwest of the epicenters. According to *Steinberg and Rabinowitz* (2003), for velocities varying with depth, receivers recording both direct and refracted waves are necessary for optimal location results. It is also noticeable for the entire sequence of 135 stations (Fig. 6b) how, unlike the test cases, the inner stations are selected first and the outermost positions last (corresponding to larger event magnitudes). However within the innermost region, the behavior is similar to that of the test cases, and stations are first
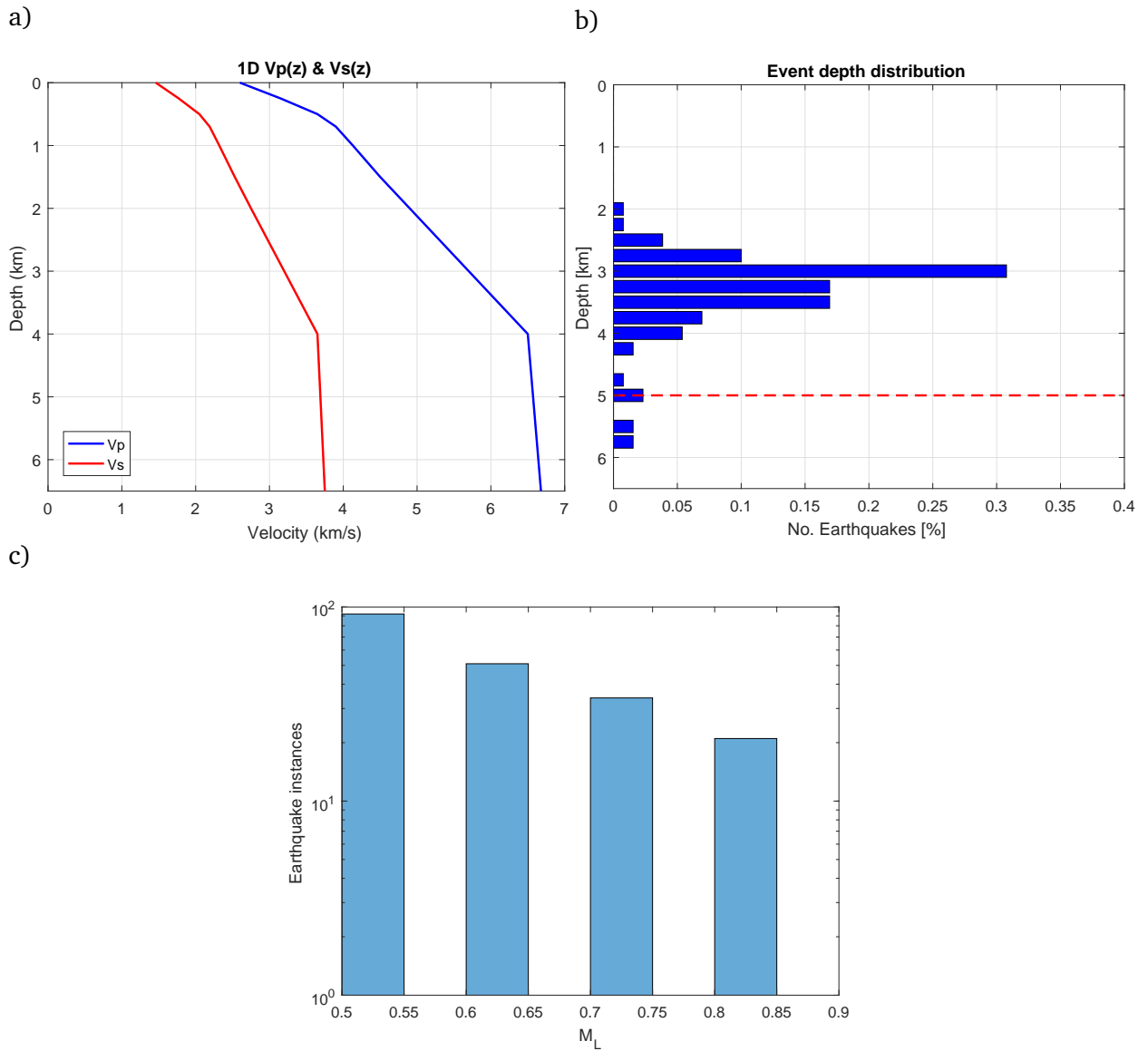
a)

b)

c)

Figure 5: Synthetic earthquake catalog specifications. a) 1D P- and S-wave velocity profiles from the SIL system (*Bjarnason et al.*, 1993). c) Event depth distribution. The red line indicate the depth above which 95 % of events are located. This limit is also known as the brittle-ductile boundary. d) Magnitude distribution of the synthetic earthquake catalog. b value = 2.16

located both close and further away from the epicenters. This behavior is the result of having clustered events, with large or entirely overlapping *deploying areas*. A possible solution to better consider the optimization of larger events is to assign them a higher weighting value γ_i (Eq. 4). However, given the network objectives to potentially detect and locate much smaller earthquakes
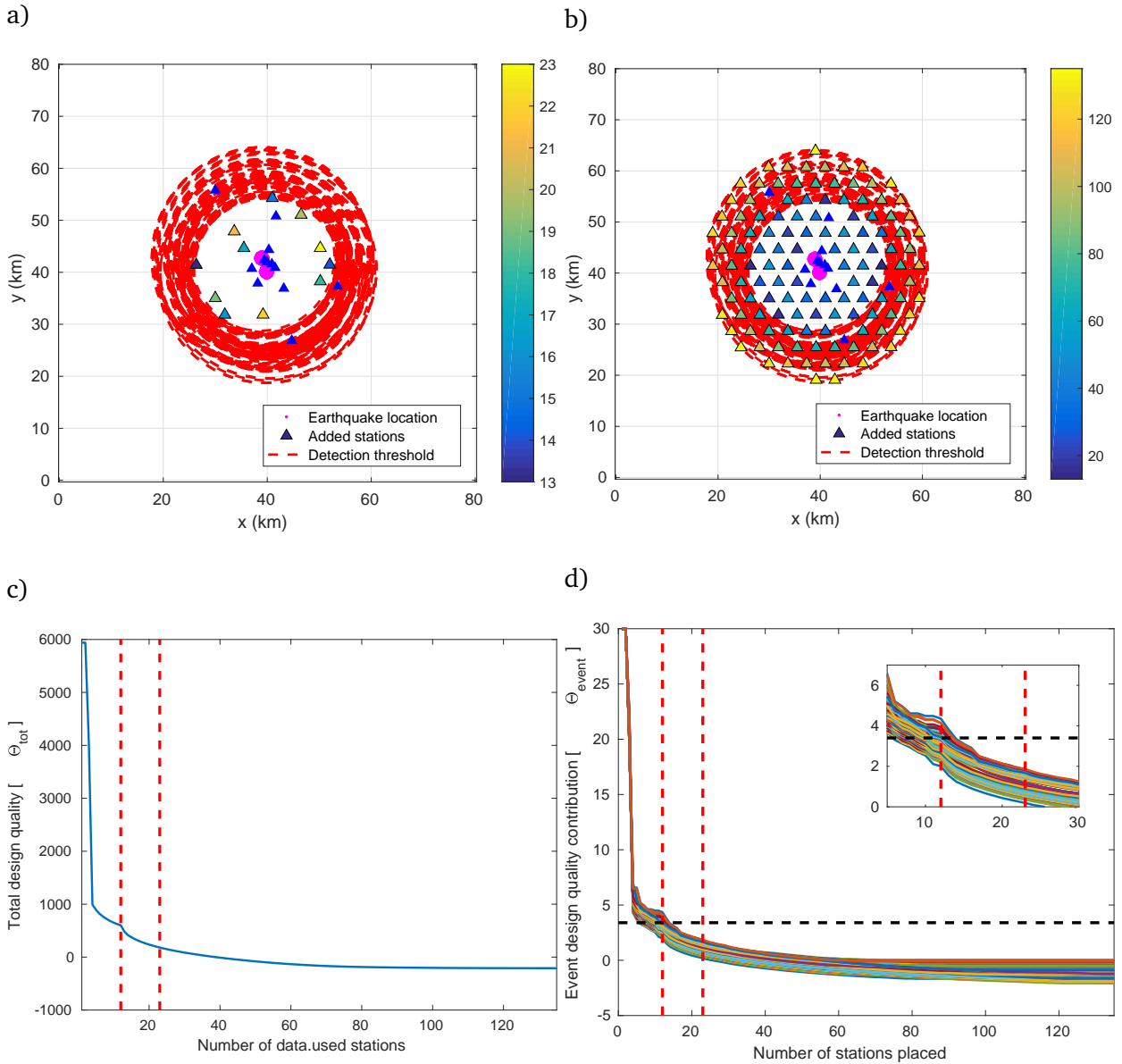
Figure 6: a) 23 station network. b) 135 station network. The colorbar expresses the order of the added stations. c) Total design quality of the survey setup after progressively adding stations. d) Design quality contribution per event for the whole experiment. The dashed red line on the left indicates the limit for the initial 12 stations, and the red line on the right the limit for a 23 station network. The horizontal dashed black line indicates the limit of $\Theta_{event} = 3.4$.

as well as the easier access to this much reduced area, we have decided to keep $\gamma_i = 1$ for the

earthquakes studied.

Similar to Test Case A, Fig. 6a presents few areas with some clustered stations (e.g. the west-

ernmost and the northern regions). Although one could argue that some of the additional stations may represent redundant information, we have decided to keep them. In this exercise we have assumed homogenous noise amplitudes and SNR, which might not be the case in reality. Therefore, by keeping the additional stations we are in some sense attempting to ensure traveltime recordings in these regions. We thus recommend to carry out a noise analysis once more seismic data becomes available and assess if and which station positions can be removed, and alternatively be placed elsewhere.

Fig. 6c and Fig. 6d depict the total Θ_{tot} and individual Θ_{event} design quality or cost curves. Notice the marked decrease in both Θ_{event} and Θ_{tot} curves after introducing only one additional sensor (station # 13). When analyzing the curves for Θ_{event}, we observe how after introducing the initial 12 stations, most curves lie below a value of 3.4. The placement of additional 11 stations results in $\Theta_{event} \leq 2$ for almost all curves. Adding many more stations would enhance the benefit much less significantly as the curves tend to flatten towards the end. As a matter of fact, Θ_{tot} stops decreasing significantly after ≈ 35 stations.

Spatial quality measure distribution

If we now take the opposite problem where the station positions are fixed and a series of hypocenters are located every 2.5 km in the x and y directions, and every 0.5 km in the z direction in a rectangular grid-like manner, we can estimate the "goodness" of the network for constraining each of these additional points by computing their corresponding quality measure Θ_{event}. Therefore this exercise consists on the observation of the network benefit for earthquakes in the region different from those in the catalog used in the design phase. Fig. 7 shows these design quality or "goodness" maps for events of magnitudes: M_L 0.5 (left column) and M_L 0.8 (right column). Uncolored areas

lie outside detectable bounds and are thus not considered for the goodness calculation. Areas marking higher values of Θ_{event} (colored in yellow) correspond to points with few readings. Conversely, low values of Θ_{event} indicate best quality and hence lower error propagation in the inversion results (Eq. 2). Notice how for both cases (3 km depth slice), the regions with low values Θ_{event} lie within the array, and is best where the network is denser especially right below the station positions in the center (Fig. 7c and Fig. 7d). This is to be expected given that these regions correspond to some of the target event locations used for the network design. The extents of the high quality area (dark blue) reach a radius of ~20 km from the epicenters shown in Fig. 4.

In a similar way, we can observe how for a E-W profile (located at approximately the domain center, y = 37.5 km) the area with best design quality has a rough semi-circular shape and is best under the denser network region, with low values (best quality) roughly reaching 10 km below the surface for both cases (Fig. 7e and Fig. 7f). For both cases, the potentially best invertible hypocenter locations match the injection and production areas, hence reaching our goal for the Theistareykir survey design with a $\Theta_{event} \approx 2$. Overall, goodness maps prove good quick tools for providing a qualitative character of the inversion errors for points across an area.

Earthquake location accuracies

As a final step, we analyze the effects of seismic array configuration on hypocenter location accuracies. For this purpose, we follow a Monte Carlo approach proposed by *Billings et al.* (1994) and calculate the standard deviation of resulting hypocentral parameters after the least-squares inversion procedure of several perturbed P- and S- wave datasets. We define these standard deviations as earthquake location accuracies. In this exercise, synthetic P- (t_P) and S-(t_S) wave arrival times were contaminated with normally distributed errors with means at 0.2 s and 0.4 s, respectively.

Considered sources correspond to the same grid points of the design quality map exercise, at a depth of 3 km. The velocity model used is shown in Fig. 5a. We subsequently invert for each dataset using a damping factor of 0.1. Initial values x_0 and y_0 were taken as the true values with normally distributed errors of 2 km, and z_0 was set to 1.5km. These values are used assuming that a previous automatic detection scheme has been used and the inversions are merely a refinement step. This is usually the procedure in microseismic problems.

Fig. 8 depicts the resulting accuracy or standard deviation maps after performing the inversions. Notice how accuracies in x and y are slightly lower than accuracies in z. This is to be expected as we have a 2D receiver configuration for a 3D problem. Events located inside the array present resulting accuracies of around 0.3 km, 0.3 km, and 0.6 km for the x, y, and z components respectively in both magnitude cases. The position errors in the inner regions (difference between true and mean inverted values in Fig. 9a and Fig. 9b) are of around half a kilometer. The areas external to the seismic network present higher accuracy values and location errors, due to the fewer travel time readings and the limited azimuthal coverage. The uncolored areas in Fig. 8 and Fig. 9 do not entirely match those provided by Fig. 7 given that only points with at least 6 data entries were inverted to avoid non-converging results.

To further study the uncertainty improvements after introducing the new stations we repeated the previous exercise, this time for the synthetic earthquake catalog used in the design phase (Fig. 5). Hence, several synthetic travel time datasets were inverted for the original 12 and final 23 station networks. Their resulting accuracy and error differences are depicted in Fig. 10. Notice how the accuracies have improved around 0.2 km for all hypocentral components and location errors. The network symmetry around the epicenters contribute to better epicentral estimates, whereas positions on top and far from them contribute to better depth estimates (*Steinberg and Rabinowitz*,

2003).

Overall, inversion results are subject to changes depending on the initial values and travel time (picking) errors. In this study we have overestimated these values, so better results should be expected with lower picking errors. Errors in the velocity model were also not accounted for in this analysis. All things considered, the resulting accuracies and errors are acceptable for the seismic network purposes, therefore validating this final 23 station array as adequate.
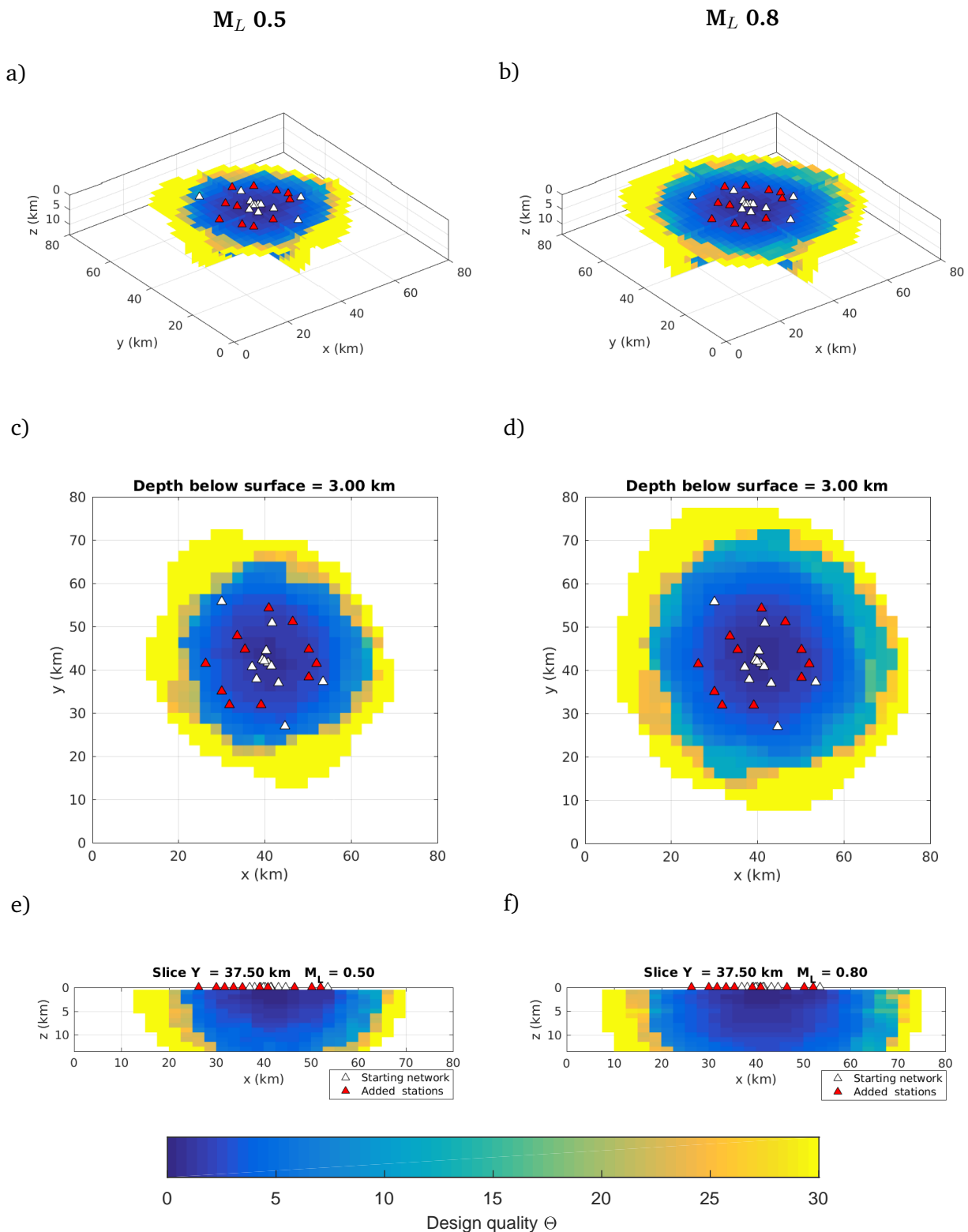
Figure 7: Measures of design quality or network goodness according to event position and magnitude. The first column indicates values associated to events of M_L 0.5, the second to M_L 0.8. White triangles mark the starting station positions. The red triangles stand for the added stations after the design experiment. a) and b) show a 3D view, c) and d) depict a depth slice at 3 km, and e) and f) an YZ profile cutting at y = 37.5 km.
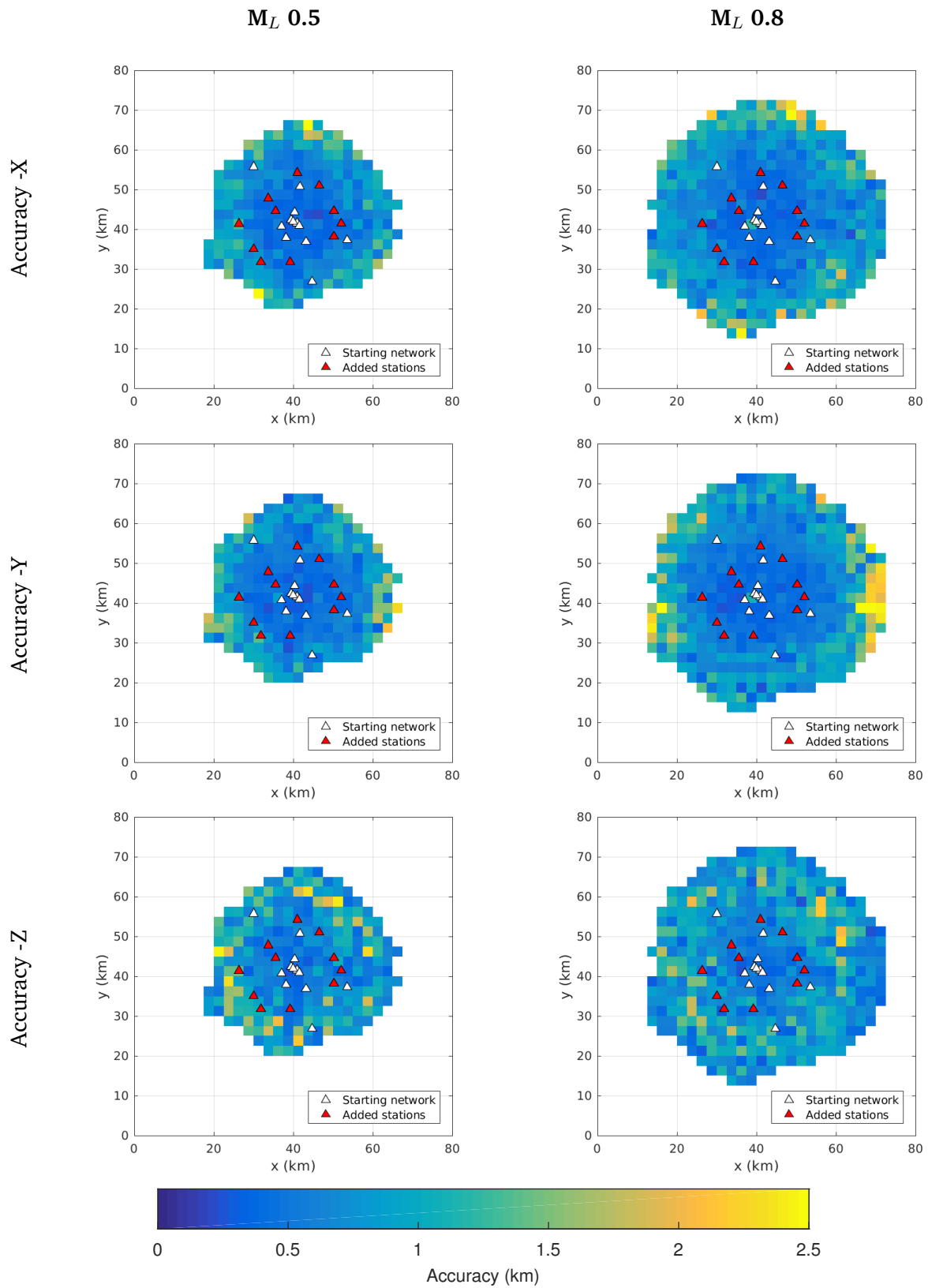
Figure 8: Accuracies of hypocentral coordinates for events at 3 km depth. The first column indicates events of M$_L$ 0.5 and the second of M$_L$ 0.8. Red triangles mark station positions.
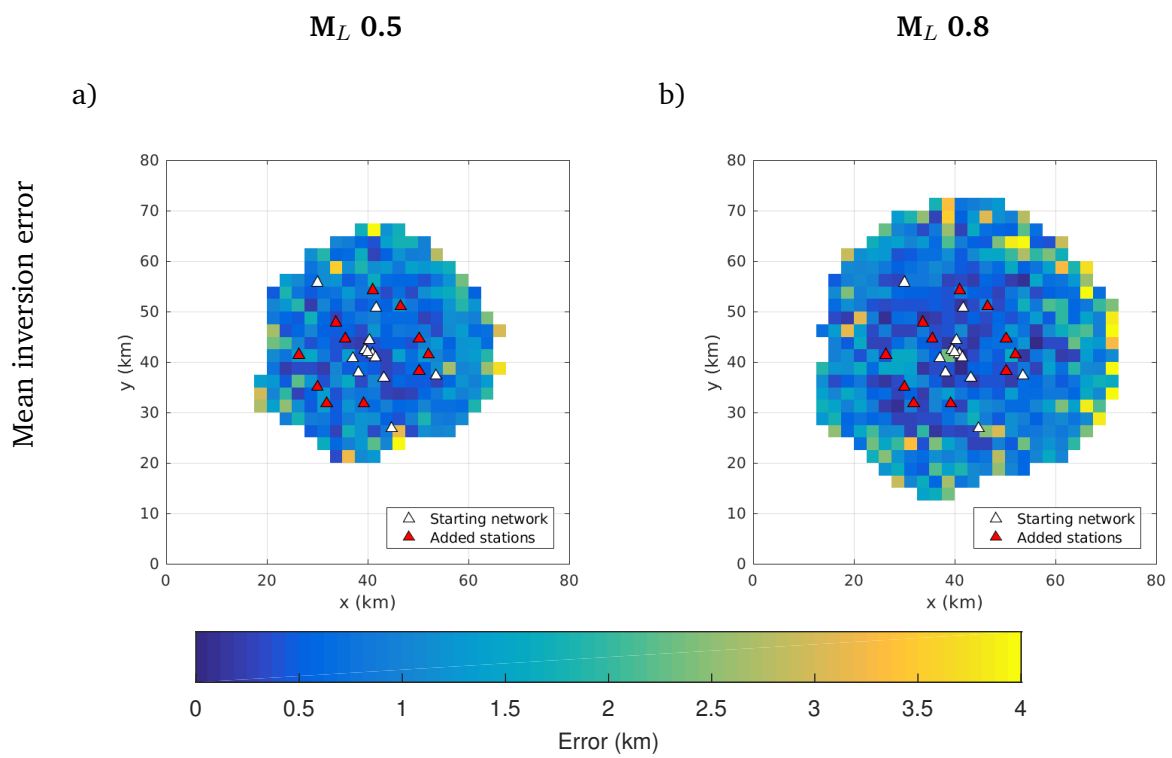
M_L 0.5

M_L 0.8

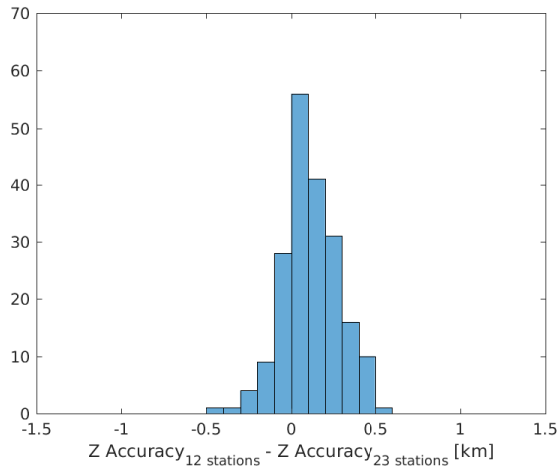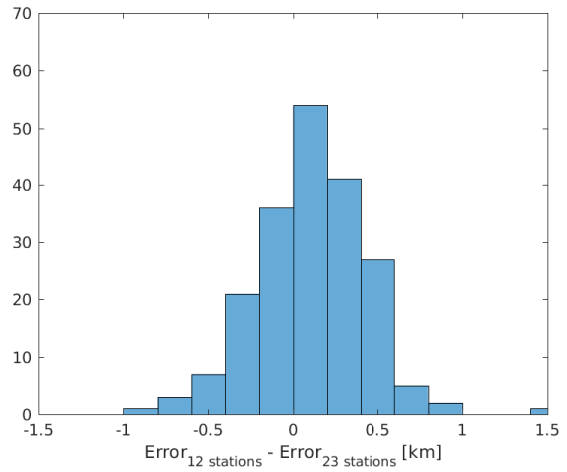**Figure 9:** Mean inversion errors for events at 3 km depth and magnitudes a) M_L 0.5 and b) M_L 0.8.
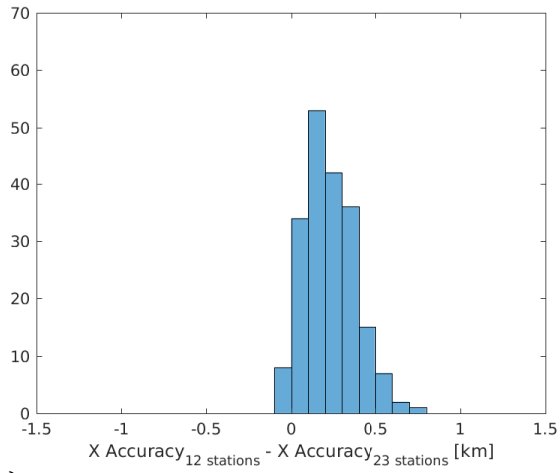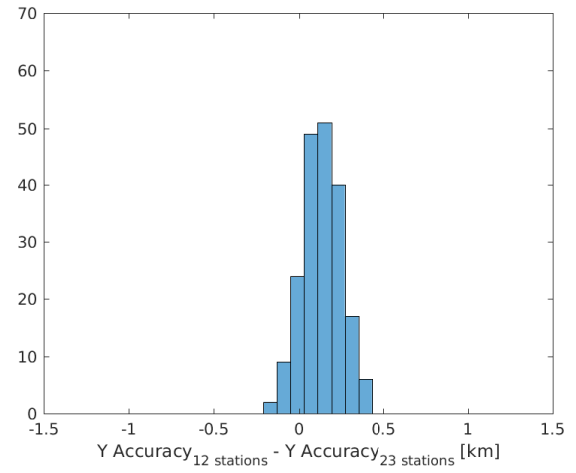
Figure 10: Location accuracy and error differences between the original (12) and final (23) station networks for events in the synthetic earthquake catalog of Fig. 5

Case study II: Reykjanes seismic data and network performance

The Reykjanes peninsula is a region located in SW Iceland (Fig. 11a) characterized by high volcanic and seismic activity resulting in a large number of high temperature geothermal areas (*Blanck et al.*, 2018, this issue). A total of 6 fields are currently being exploited in this region and are associated to four NE-SW oriented fissure swarms connected to 4 different volcanic systems (*Harðardottir et al.*, 2009). Particularly the Reykjanes field located at the tip of the peninsula has a capacity of 100 MWe (*Friðleifsson et al.*, 2018, this issue).

Within the framework of the IMAGE project (Integrated Methods for Advanced Geothermal Exploration) a passive seismic array consisting of 86 on-land sensors and OBS distributed on and around the peninsula was used to monitor the seismicity, and enhance and develop existing and new passive seismic techniques for imaging geothermal fields (Fig. 11a). The array consisted of 30 temporary on-land seismometers distributed in a concentric fashion around the Reykjanes peninsula, 26 OBS surrounding the peninsula, 8 seismic stations handled by ISOR for the permanent monitoring of the Reykjanes geothermal field, 15 stations of the Czech Academy of Science (CAS) used for monitoring the Krýsuvík geothermal system, and 7 permanent stations handled by the IMO as part of the national seismic network (*Blanck et al.*, 2018, this issue). The array recorded from march 2014 to august 2015, and the resulting dataset was used to study the regional seismicity and structures by means of re-localization and focal mechanism analysis (*Blanck et al.*, 2018, this issue), travel time tomography (*Jousset et al.*, 2018, this issue), ambient noise analysis (*Weemstra et al.*, 2016), and seismic interferometry (*Verdel et al.*, 2016; *Martins et al.*, 2018, this issue). *Einarsson et al.* (2018, this issue) additionally analyzed the natural and exploitation related stress field changes of the region.
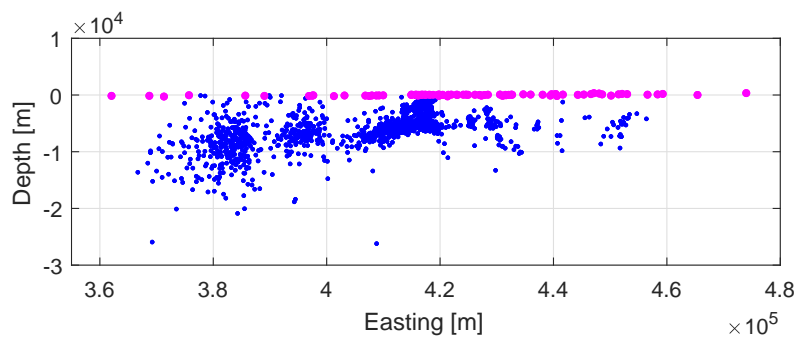
a)
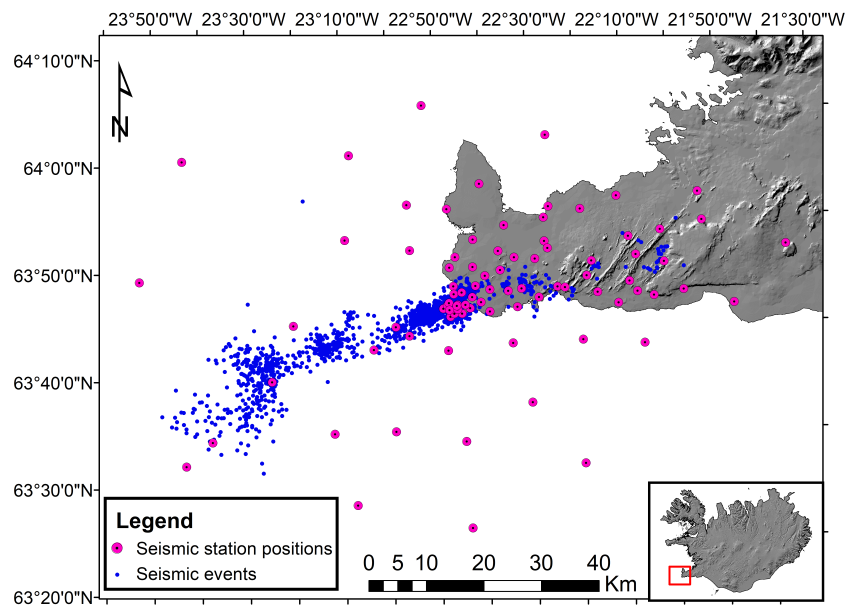
b)

Figure 11: a) Seismic events, seismometers, and OBS positions. b) EW profile. Topography is ignored for its rather small variation.

Seismic Network quality

A total of 2066 earthquakes were automatically detected with an STA/LTA approach after which P- and S- wave arrivals were picked manually. An initial earthquake location was carried out by *Blanck et al.* (2018, this issue) using the 1D SIL velocity model (*Bjarnason et al.*, 1993), and later relocated the hypocenters using the model derived by *Jousset et al.* (2018, this issue) shown in Fig.

12a. For the exercise of qualifying the network design we reduce the seismic catalog to account only for events placed within the network and located with at least 3 P- and 3 S- wave picks. The remaining 1981 seismic events are displayed as blue points in Fig. 11a and Fig. 11b. Seismic events are mostly distributed along the mid-ocean ridge, with the majority located close to the Reykjanes peninsula tip (third cluster on the right). These earthquakes reach a maximum depth of around 6km, marking the brittle-ductile boundary of that region in accordance to a previous study by *Kristjánsdóttir* (2013). Fig. 12b depicts the maximum station-event distance relationship per earthquake needed to construct theoretical *deploying areas*. Notice how a significant number of events reach a maximum distance of around 10 km corresponding, in a large degree, to events located under the Reykjanes peninsula.
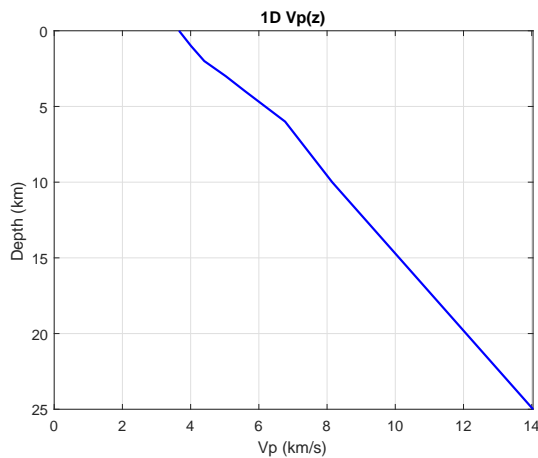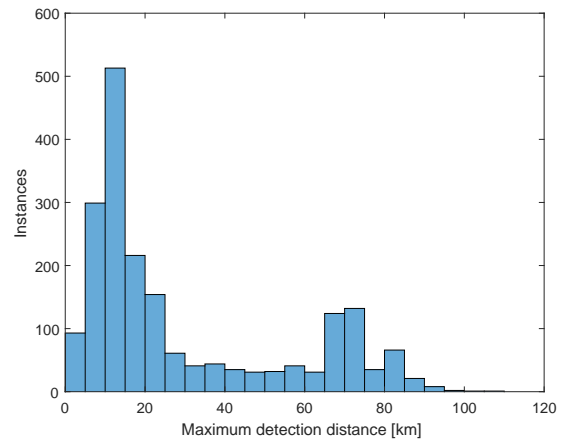
a)   b)

Figure 12: a)1D Vp velocity model. (*Jousset et al.*, 2018, this issue). b) Maximum detection distances.

To assess the quality of the Reykjanes seismic array with respect to the located earthquakes we ran the DSSD algorithm using the 86 station positions as hypothetic "location points". Fig. 13a illustrates the resulting order of importance of the receiver positions. As in previous design exercises the routine has primarily selected stations located above most seismic events (close to

the Reykjanes peninsula tip), followed by some outer stations. Fig. 13b and Fig. 13c depict design qualities Θ_{tot} and Θ_{event}, respectively. Like before, cost curves decrease progressively and become almost flat with the total number of stations. The quality Θ_{event} limit for the total 86 sensors range from -1.83 to 8.4, corresponding to an average per event of 2.35 obtained from Θ_{tot}. If we move to 80% of the seismic stations (71 sensors) the range of Θ_{event} is of -1.60 to 8.4 and a mean 2.41 per event from Θ_{tot}. This means that some ~18 stations could be spared to provide similar confidence ellipsoid volumes, therefore hinting the importance of a preliminary survey design experiment to optimize costs. In a similar sense, these theoretical results highlight the importance of some of the OBS deployed (in dark blue). OBS deployment was originally not contemplated in the project but by this study, their eventual placement is justified.

Fig. 14 shows the resulting accuracies and expected errors of inverted datasets associated to smaller arrays. The Vp/Vs ratio was taken at 1.78 (*Blanck et al.*, 2018, this issue). P- and S- wave synthetic datasets were contaminated with normal distributed errors with means at 0.15 s and 0.30 s, respectively, and later inverted to obtain hypocentral parameter accuracies and errors. It is clear once more how accuracies seem to remain stable from 80% stations on. The 86 station network was nevertheless chosen to account for alternative seismic techniques such as ambient noise tomography (*Martins et al.*, 2018, this issue). For this analysis we have once more ignored effects of different source mechanisms, heterogeneous noise distribution, and sensor installation quality, though we encourage further studies accounting this additional information.
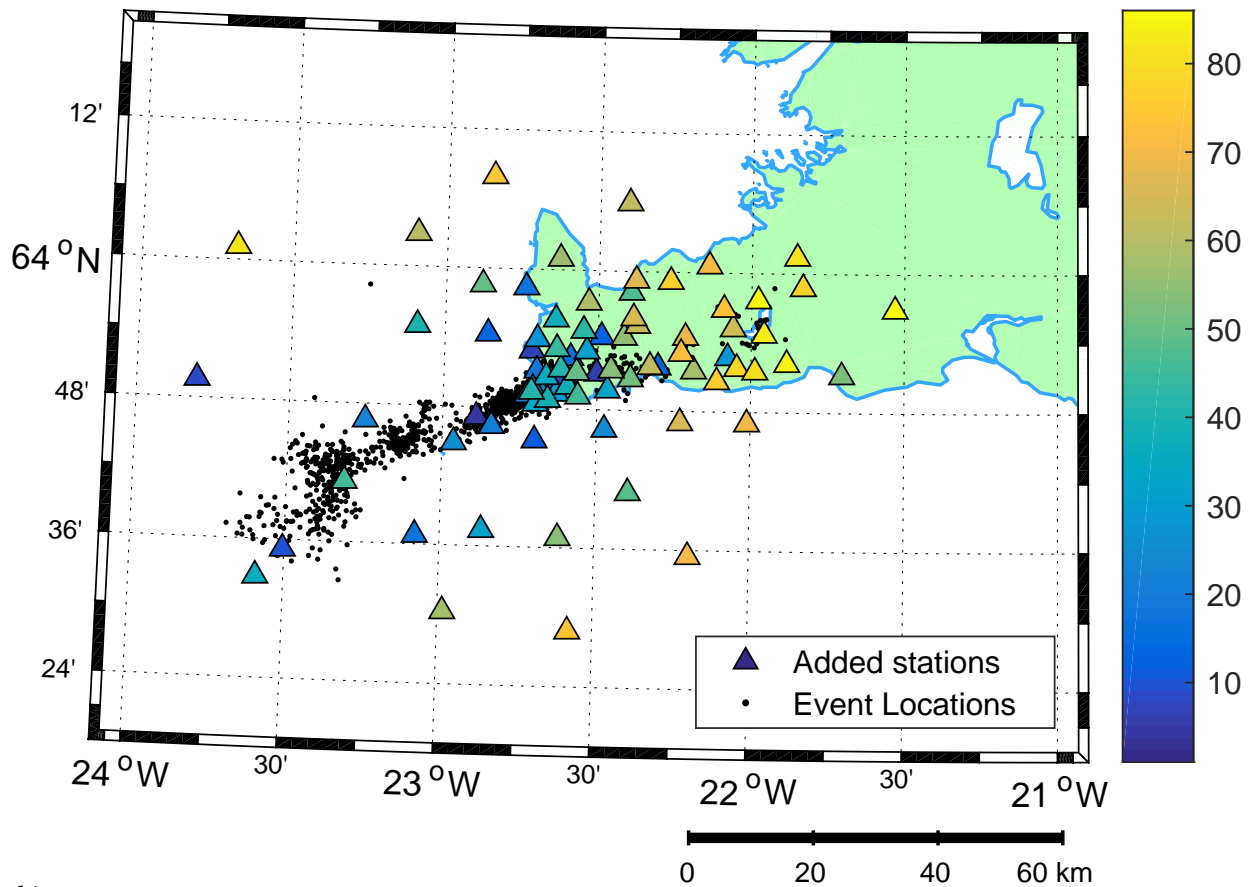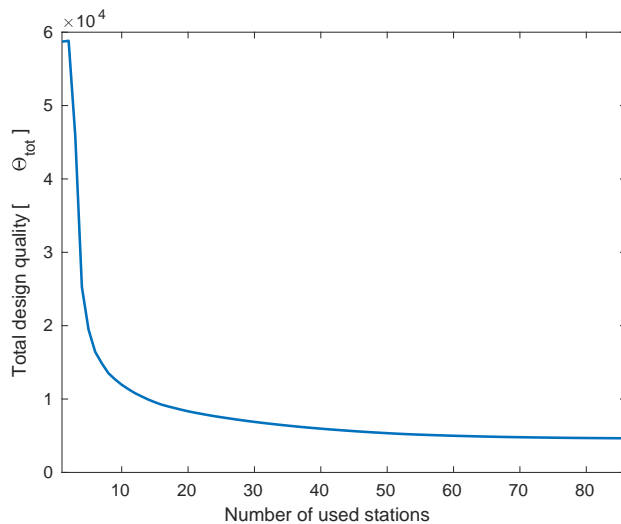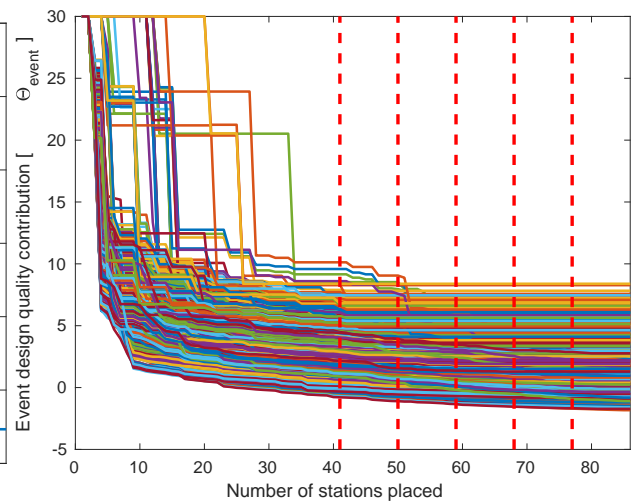
Figure 13: Reykjanes network quality. a) Order of importance of the Reykjanes seismic stations. b) Total design quality of the survey setup after progressively adding stations. c) Design quality contribution per event for the whole experiment. The dashed red lines indicate the limits of 50%, 60%, 70%, 80%, and 90% stations.
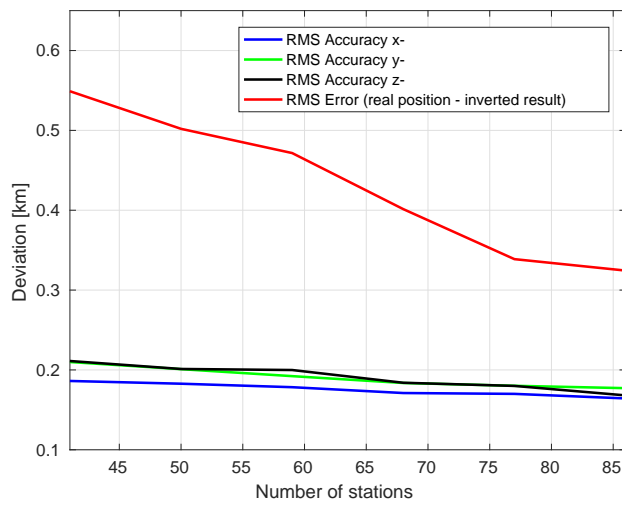
Figure 14: Location accuracies given by a station number reduction

Discussion

The linearized sequential survey design hereby explored is a rather simple method for building and qualifying seismic networks; however, it presents some drawbacks that must be addressed to obtain optimal designs.

D-optimality

Results using the chosen objective function Θ are very influenced by overlapping deploying areas, favoring them when these are very large. While this behavior could favor locating receivers that record as many possible events, it could also compromise the optimization of single events. It is therefore of importance to first identify main target earthquakes to allocate them high weighting factors γ_i (Eq. 4) prior to design. When no apriori accurate locations are known, an experiment similar to the one shown in Fig. 3 can be used.

Another issue that must be considered when using the *D-criterion* is station clustering. This phenomena is particularly likely in problems involving large number of stations to be placed in reduced *deplyoing areas* (e.g. Case I), or when failing to place stations right above a studied epicenter (e.g. Test Case A). Station clustering is the consequence of Θ ignoring model error correlations. One way to account for this correlation is by introducing an inter-station distance weight as performed by *Hardt and Scherbaum* (1994). In this work we decided to overlook this correction, and interpret the clustering as regions of importance instead (e.g. *Kraft et al.*, 2013).

Linearized destruction sequential survey design

In this work, we have explored a linearized destruction sequential survey design algorithm for its robustness, simplicity, and its ability to obtain optimal network configurations. A big advantage of sequential routines is their ability to quickly take into account changes of station positions (had they not been placed exactly at theoretical locations) and recompute design experiments for new geometries. Additionally, sequential survey design allows for an intuitive analysis of benefit/cost relations.

However, one disadvantage of destruction schemes comes with the computational expense when dealing with large number of earthquakes and candidate station positions. With destruction techniques one has to build the entire sequence/order of stations to obtain the position of even a few of them. Construction algorithms on the other hand provide much faster and cheaper results however possibly compromising global optimality. Given that at each iteration a new station is placed, these algorithms require only as many iterations as stations needed. This technique could then provide a framework for potential design-during-deployment. However, one main drawback of construction design is its need for good initialization (setting the first station position) which can seriously influence design optimality. Another sequential design option with better global optimality is exchange design (*Coles and Curtis*, 2011b). These algorithms scan through all observation points and replace station positions that extremize the objective function. Although quite robust in achieving global optimality, this routine requires twice as much computation than the previous two, given that each iteration needs two steps: construction and deletion.

Overall, although global optimality cannot be guaranteed with linearized sequential design approaches, these techniques provide fast optimal designs nonetheless. The simplicity of these routines is particularly useful in cases that require quick designs like post-earthquake aftershock

studies, or simply building quick temporal networks. All the same, for cases requiring permanent stations or extended monitoring we recommend alternative design approaches such as global search algorithms like simulated annealing, and/or non-linear experimental design. Although some of these schemes may represent higher computational demands, they do ensure global optimality.

Detectability

Another key aspect to address in survey design is detectability. Detectability is very roughly considered in this work, however it is critical for defining candidate points for deployment. In our experiments we have considered homogeneous noise levels and SNR. In reality, these values are laterally variant and are very much site-specific. Authors like *Kraft et al.* (2013) for example calculated a first order ambient noise model to observe the lateral noise variations in Switzerland. Then, they compared these values with phase amplitudes modeled using Brune's source model (*Brune*, 1970, 1971) to determine the detecting stations. This procedure was possible given the availability of prior seismic data for this region. In practice, detailed knowledge of lateral velocity variations, anisotropy, attenuation, site-specific noise, SNR levels, etc. is largely unknown in unstudied areas. Hence the need of a seismic array in the first place. Inevitably, we would in many cases rely on oversimplified models and assumptions that could potentially lead to suboptimal designs. For this reason we recommend repeating optimization experiments once more information on the target site becomes available, especially in cases requiring permanent or extended monitoring. Survey design could in these cases be regarded as an iterative procedure that improves with our knowledge of the target area.

Design and qualification of seismic arrays

Case study I offers a real case for constructing a small microseismic array in Theistareykir geothermal field. This case however considers very clustered events as location targets which directly affects station placement due to large deploying areas overlap. Nonetheless we have judged that the region considered is appropriate for fieldwork conditions and therefore decided not to assign higher γ_i values for larger events. With the introduced routine we have constructed a 23 station network. The network performance was later tested by carrying out several Monte Carlo experiments to calculate standard deviations of the inversion results with theoretical noisy data. Monte Carlo experiments however can be very computationally expensive. For this reason we discussed the use of "goodness maps" which are simply the spatial distribution of quality measure Θ. These maps are much faster to compute and can qualitatively reveal the extents of areas where events would be better constrained by the network.

Case study II uses the same design scheme to qualify an existing seismic array at the Reykjanes peninsula. The algorithm is applied in the same fashion as in Case I, however with the deployed stations as potential placement points. This approach results in the construction of a station order of importance. We later tested the effects of removing least important stations in the resulting location uncertainties. It was noticeable for the Reykjanes network, that we would arrive to similar location uncertainties with only 71 stations out of 86. These findings are of critical importance especially with constrained project budgets, hinting the value of experimental survey design prior to deployment. On a similar tone, many seismic experiments require moving stations to different positions at some point in time. Therefore similar analysis can help identify which stations are crucial to the experiment and which can be moved without affecting location uncertainties significantly.

Conclusions

We have successfully constructed and applied a DSSD algorithm for designing new optimized seismic networks, and qualifying existing ones for geothermal studies in the framework of sequential survey design based on the *D-criterion*. The DSSD scheme hereby explored uses a 1D velocity model for sensitivity computations, and was first tested with simple test-cases where concepts like benefit and cost were introduced. The routine was then applied to two case studies, one for designing (Theistareykir) and a second one for qualifying (Reykjanes) an existing seismic array.

After constructing a synthetic earthquake catalog in accordance with previously observed seismic data, the Theistareykir network was augmented with the DSSD algorithm, from 12 to 23 sensors, reaching hypocentral accuracies of around ∼0.5 km for normally distributed picking errors of mean 0.2 s (for t_P) and 0.4 s (for t_S).

Finally the Reykjanes network was tested with the same algorithm to observe whether its design was adequate for the recovered earthquake catalog. From the design quality values it became apparent that up to ∼18 stations could be spared for the survey, or conversely relocated for better results. It is therefore of importance to conduct a survey design experiment prior to deployment to obtain best possible location results. In this study we have not considered the effects of variable seismic noise, for which a better detectability study could be carried out in the future to refine results. Another interesting topic for future research is the building of a multi-purpose network design for both velocity model and seismic event locations, and the use of alternative non-linear quality metrics.

Acknowledgements

1 References

Aki, K., and P. Richards (1980), Quantitative seismology: Theory and methods, *WH Freeman & Co.*

Ármannsson, H. (2008), The Theistareykir geothermal system, northeast Iceland. Case History, *Presented at Short Course III on exploration for Geothermal Resources*.

Beyreuther, M., R. Barsch, L. Krischer, T. Megies, Y. Behr, and J. Wassermann (2010), Obspy: A python toolbox for seismology, *SRL*, *81*(3), 530–533.

Billings, S., M. Sambridge, and B. Kennett (1994), Errors in hypocenter location: picking, model, and magnitude dependence, *Bulletin of the Seismological Society of America*, *84*(6), 1978–1990.

Bjarnason, I. T., W. Menke, O. G. Flóvenz, and D. Caress (1993), Tomographic image of the Mid-Atlantic Plate Boundary in southwestern Iceland, *J. Geophys. Res.*, *98*, 6607–6622.

Blanck, H., K. Ágústsson, and K. Gunnarsson (2017), Seismic monitoring in Theistareykir, Krafla and Námafjall, *Landsvirkjun Report*, *LV-2017-046*.

Blanck, H., P. Jousset, G. P. Hersir, K. Ágústsson, and O. G. Flóvenz (2018), Analysis of seismological data on Reykjanes Peninsula, SW-Iceland, *Journal of Volcanology and Geothermal Research*.

Bormann, P. (1998), Conversion and comparability of data presentations on seismic background noise, *J. Seismol.*, *2*, 37–45.

Brune, J. B. (1970), Tectonic stress and spectra of seismic shear waves from earthquakes, *J. geophys. Res.*, *75*(26), 4997–5009.

Brune, J. B. (1971), Correction to "Tectonic stress and spectra of seismic shear waves from earthquakes", *J. geophys. Res.*, *75*(20), 5002.

Buland, R. (1976), The mechanics of locating earthquakes, *Bull. seism. Soc. Am.*, *66*(1), 173–187.

Cesca, S., and F. Grigoli (2015), Full waveform seismological advances for microseismic monitoring, *Advances in Geophysics*, *56*.

Chaloner, K., and I. Verdinelli (1995), Bayesian experimental design: A review, *Statistical Science*, *10*(3), 273–304.

Coles, D., and A. Curtis (2011a), Efficient nonlinear Bayesian survey design using D_N optimization, *Geophysics*, *76*(2), Q1–Q8.

Coles, D., and A. Curtis (2011b), A free lunch in linearized experimental design?, *Computers and Geosciences*.

Cuenot, N., C. Dorbath, and L. Dorbath (2008), Analysis of the microseismicity induced by fluid injections at the EGS Site of Soultz-sous-Forêts (Alsace, France): Implications for the characterization of the geothermal reservoir properties, *Pure and Applied Geophysics*, *165*, 797–828.

Curtis, A. (1999), Optimal experiment design: Cross-borehole tomographic examples, *Geophysics Journal International*, *136*, 637–650.

Curtis, A. (2004), Theory of model-based geophysical survey and experimental design. part a—linear problems, *The Leading Edge*, *23*, 997–1004.

Curtis, A., A.Michelini, D. Leslie, and A. Lomax (2004), A deterministic algorithm for experimental design applied to tomographic and microseismic monitoring surveys, *Geophysical Journal International*, *157*, 595–606.

Dyer, B. C., U. Schanz, and T. Spillman (2008), Microseismic imaging of a geothermal reservoir stimulation, *The Leading Edge*, *27*(7).

Eberhart-Phillips, D. (1990), Three-dimensional P and S velocity structure in the Coalinga region, California, *Journal of Geophysical Research*, *95*(B10), 15,343–15,363.

Einarsson et al. (2018), title pending, *Journal of Volcano and Geothermal Research*.

Ellsworth, W. L. (1977), Three dimensional velocity structure of the crust and mantle beneath the island of Hawaii, *PhD Dissertation. MIT, Cambridge U.S.A*, p. 327.

Flinn, E. A. (1965), Confidence region and error determinations for seismic event location, *Rev. Geophys.*, *3*(1), 157–185.

Foulger, G., R. Long, and P. Einarsson (1983), Implosive earthquakes at the active plate boundaries in Iceland, *Nature*, *337*, 640–642.

Friðleifsson et al. (2018), title pending, *Journal of Volcanology and Geothermal Research*.

Geiger, L. (1912), Probability method for the determination of earthquake epicenters from the arrival time only, *Bulletin of St. Louis University*, *8*, 60–71.

Glenn, W. E., and S. H. Ward (1976), Statistical evaluation of electrical sounding methods, part 1: Experimental design, *Geophysics*, *41*, 1207–1221.

Gomberg, J. S., K. M. Shedlock, and S. W. Roecker (1990), The effect of s-wave arrival times on the accuracy of hypocenter estimation, *Bull Seism. Soc. Am.*, *80*(6), 1605–1628.

Guest, T., and A. Curtis (2009), Iteratively constructive sequential design of experiments and surveys with nonlinear parameter-data relationships, *Journal of Geophysical Research*, *114*.

Hardt, M., and F. Scherbaum (1994), The design of optimum networks for aftershock recordings, *Geophysics Journal International*, *6*.

Harðardottir, V., K. L. Brown, T. Friðriksson, J. W. Hedenquist, M. D. Hannington, and S. Thórhalsson (2009), Metals in deep liquid of the Reykjanes geothermal system, southwest Iceland: implications for the composition of seafloor black smoker fluids, *Geology*, *37*, 1103–1106.

Jakobsdóttir, S. S. (2008), Seismicity in Iceland: 1994-2007, *Jökull*, *58*.

Jones, A. G., and J. H. Foster (1986), An objective real-time data-adaptive technique for efficient model resolution improvement in magnetotelluric studies, *Geophysics*, *51*, 90–97.

Jousset, P., C. Haberland, K. Bauer, and A. K. (2011), Detailed structure of the Hengill geothermal volcanic complex, Iceland inferred from 3-D tomography of high dynamic broadband seismological data, *Elsevier Geothermics*.

Jousset, P., et al. (2018), Image geothermal field structure prior to drilling: insights from travel time seismic tomography in Reykjanes, SW Iceland, *Journal of Volcanology and Geothermal Research*.

Jousset et al. (2018), Title pending, *EGU conference*.

Kao, H., and S. J. Shan (2007), Rapid identification of earthquake rupture plane using source-scanning algorithm, *Geophysical Journal International*, *168*, 1011–1020.

Kijko, A. (1977), An algorithm for the optimum distribution of a regional seismic network-I, *Pageoph.*, *115*, 999–1009.

Kirkpatrick, S., C. Gelatt, and M. Vecchi (1983), Optimization by simulated annealing, *Science*, *220*, 671–680.

Kissling, E., W. L. Ellsworth, D. Eberhard-Phillips, and U. Kradolfer (1994), Initial reference models in local earthquake tomography, *J.Geophys. Res*, *99*, 19,635–19,646.

Kraft, T., A. Mignan, and D. Giardini (2013), Optimization of a large-scale microseismic monitoring in northern Switzerland, *Geophysical Journal International, 195,* 474–490.

Kristjánsdóttir, S. (2013), Microseismicity in Krýsuvík Geothermal Field. SW Iceland, from May to October 2009, *Master thesis*.

Landsvirkjun (2016), Geothermal power station at Theistareykir: Energy utilisation in Northeast Iceland, *Landsvirkjun 2016 newsletter*.

Lee, W. H. K., and S. W. Stewart (1981), Principles and applications of microearthquake networks, *Office of earthquake studies. U.S.G.S. Academic Press*.

Lees, J. (2004), Seismic imaging of fractures at Krafla, Iceland, *International Federation of Digital Seismograph Networks. Other/Seismic Network. 10.7914/SN/XY_2004*.

Levenberg, K. (1944), A method for the solution of certain non-linear problems in least squares, *Q. Appl. Math, 2,* 164–168.

Lomax, A. (2005), A reanalysis of the hypocentral location and related observations for the great 1906 California Earthquake, *Bull. Seism. Soc. Amer., 95,* 861–877.

Majer, E. L., R. Baria, M. Stark, S. Oates, J. Bommer, B. Smith, and H. Asanuma (2007), Induced seismicity associated with enhanced geothermal systems, *Geothermics, 36,* 185–222.

Marquardt, D. W. (1963), An algorithm for least-squares estimation of nonlinear parameters, *J. Soc. Ind. Appl. Math., 11,* 431–441.

Martins, J. E., C. Weemstra, E. Ruigrok, A. Verdel, P. Jousset, and G. P. Hersir (2018), 3D S-wave velocity of the Western Reykjanes peninsula, Iceland, from ambient-noise tomography, *Journal of Volcano and Geothermal Research*.

Maurer, H., and D. E. Boerner (1998), Optimized and robust experimental design: a non-linear application to em sounding, *Geophysics Journal International, 132*, 458–468.

Maurer, H., A. Curtis, and D. Boerner (2010), Recent advances in optimized geophysical survey design, *Geophysics, 75*(5).

McMechan, G. A. (1982), Determination of source parameters by wavefield extrapolation, *Geophysical Journal of the Royal Astronomical Society, 71*, 613–628.

McNamara, D. E., and R. P. Buland (2004), Ambient noise levels in the continental united states, *Bulletin of the Seismological Society of America, 94*(4), 1517–1527.

Menke, W. (2012), Geophysical data analysis: discrete inverse theory, *Elsevier/Academic Press.*

Michelini, A. (1995), An adaptative-grid formalism for traveltime tomography, *Geophysics Journal International, 121*, 489–510.

Mitchell, T. J. (1974), An algorithm for construction of "D-optimal" experimental design., *Technometrics, 16*, 2013–210.

Nuber, A., E. Manukyan, and H. Maurer (2017), Optimising measurement geometry for seismic near-surface full waveform inversion, *Geophysical Journal International, accepted manuscript.*

Pavlis, G. L. (1986), Appraising earthquake hypocenter location errors: a complete, practical approach for single-event locations, *Bull. Seism. Soc. Am., 76*, 1699–1717.

Persson, P.-O., and G. Strang (2004), A simple mesh generator in MATLAB, *SIAM J. Applied Math, 46*(2), 329–345.

Philips, W. S., J. T. Rutledge, and L. House (2002), Induced micro-earthquake patterns in hydrocarbon and geothermal reservoirs: six case studies, *Pure and Applied Geophysics, 159*, 345–369.

Podvin, P., and I. Lecomte (1991), Finite difference computations of travel-times in very contrasted velocity models: a massive parallel approach and its associated tools, *Geophys. J. Int*, *105*, 271–284.

Rabinowitz, N., and D. Steinberg (1990), Optimal configuration of a seismographic network: a statistical approach, *Bull. Seism. Soc. Am.*, *80*, 187–196.

Roecker, S. W. (1981), Seismicity and tectonics of the Pamir-Hindu Kush region of central Asia, *PhD Dissertation. MIT, Cambridge, U.S.A.*, p. 140.

Sambridge, M. S., and B. L. N. Kennett (1986), A novel method of hypocenter location, *Geophys. J. R. astr. Soc.*, *87*, 679–697.

Sambridge, M. S., and B. L. N. Kennett (2001), Seismic event location: nonlinear inversion using a neighbourhood algorithm, *Pure applied Geophysics*, *158*, 241–257.

Shimsoni, Y., E. Mizrachi, D. M. Steinberg, and N. Rabinowitz (1992), OPTINET: A computer program for designing the optimal configuration of a seismographic network, *Inst. Petroleum Res. and Geophys.,*, *Report No 321/47/91(4)*.

Steinberg, D. M., and N. Rabinowitz (2003), Optimal seismic monitoring for event location with application to on site inspection of the comprehensive nuclear test ban treaty, *Metrika*, *58*(1), 31–57.

Steinberg, D. M., N. Rabinowitz, Y. Shimshoni, and D. Mizrachi (1995), Configuring a seismographic network for optimal monitoring of fault lines and multiple sources, *Bulletin of the Seismological Society of America*, *85*(6), 1847–1857.

Surono, M., et al. (2012), The 2010 explosive eruption of Java's Merapi volcano - a '100-year' event, *Journal of Volcanology and Geothermal Research, Elsevier, 241-242*, 121–135.

Sveinbjornsdottir, A. E., H. Ármannsson, M. Ólafsson, F. Óskarsson, S. Markússon, and S. Magnus-dóttir (2013), The Theistareykir geothermal field, NE Iceland. isotopic characteristics and origin of circulating fluids, *Procedia Earth and Planetary Science, 7*, 822–825.

Tarantola, A. (2005), Inverse problem theory and methods for model parameter estimation, *Society for Industrial and Applied Mathematics, Philadelphia*.

Tester, J. W., et al. (2006), The future of geothermal energy – impact of enhanced geothermal systems (EGS) on the United States in the 21st century, *MIT - Massachusetts Institute of Technology, Cambridge, MA*.

Thurber, C. (1992), Hypocenter-velocity structure coupling in local earthquake tomography, *Phys. Earth Planet Inter., 75*(1), 55–62.

Uhrhammer, R. (1980), Analysis of small seismographic station networks, *Bull. Seism. Soc. Am., 70*, 1369–1379.

Valtonen, O., M. Uski, A. Korja, T. Tiira, and J. Kortström (2013), Optimal configuration of a micro-earthquake network, *Advances in Geosciences, 33*, 33–36.

Verdel, A., et al. (2016), Reykjanes ambient noise reflection interferometry., *Proceedings of the European Geothermal Congress 2016, Strasbourg, France*.

Weemstra, C., A. Obermann, A. Verdel, B. Paab, H. Blanckk, E. A. Gudnason, G. P. Hersir, P. Jousset, and O. Sigurdsson (2016), Time-lapse seismic imaging of the Reykjanes geothermal reservoir, *Proceedings of the European Geothermal Congress 2016, Strasbourg, France*.

Wilkinson, P., P. Meldrum, J. Chambers, O. Kuras, and R. Ogilvy (2006), Improved strategies for
the automatic selection of optimized sets of electrical resistivity tomography measurement con-
figurations, *Geophysical Journal International, 167,* 1119–1126.

Witten, B., and B. Artman (2011), Signal-to-noise estimates of time reverse images, *Geophysics*,
76(2), MA1–MA10.